Mottl, M.J., Davis, E.E., Fisher, A.T., and Slack, J.F. (Eds.), 1994
Proceedings of the Ocean Drilling Program, Scientific Results, Vol. 139

4. PLANKTONIC FORAMINIFERAL BIOSTRATIGRAPHY AND PALEOCEANOGRAPHY OF LATE QUATERNARY TURBIDITE SEQUENCES AT HOLES 856A, 857A, AND 857C, LEG 139[1]

Charlotte A. Brunner[2]

ABSTRACT

Late Quaternary planktonic foraminiferal biostratigraphy and paleoceanography were examined at two sites from the east margin of Middle Valley of the northern Juan de Fuca Ridge. Calcareous microfossils are abundant and well preserved in the upper sequences where thermal and hydrothermal alteration is minimal and where deposition occurred after sites were tectonically raised above the turbidite plain of the axial valley. Approximately 200 samples were examined to determine depositional style and foraminiferal content including a census of planktonic foraminifers. Approximately 60% of the samples contain turbiditic material, so paleontologic interpretations must be made with caution.

Ocean Drilling Program (ODP) Holes 856A and 857A contain abundant foraminifers above 52 and 85 mbsf, respectively. The fossiliferous sequences are divided into four informal coiling direction zones based on the species *Neogloboquadrina pachyderma* (Ehrenberg) and numbered from 1 to 4 from top to bottom of the sequences. Coiling direction zones 1 and 3 contain <90% sinistral forms and include the lower part of the present and penultimate interglacial periods and perhaps part of the glacial termination. Coiling direction zones 2 and 4 contain >90% sinistral forms and span most of the last two glacial periods. The bases of coiling direction zones 1 and 3 define two datum levels tentatively dated at 11,000 and 125,000 yr ago, respectively.

Cluster analysis identified three assemblages: a subarctic assemblage, a transitional assemblage, and a subarctic dissolution assemblage. The subarctic dissolution assemblage occurs infrequently and sporadically throughout the unaltered glacial intervals in Holes 856A and 857A. In contrast, the dissolution assemblage dominates Hole 856A below 22 mbsf and is related to calcite precipitation driven by hydrothermal processes. The transitional assemblage appears in coiling direction zone 3 and records the close approach of the subpolar boundary to the ODP Leg 139 locale during the penultimate interglacial period. The subpolar boundary remained south of the study site at approximately 48°30′N latitude throughout the late Quaternary.

INTRODUCTION

The nominal objectives of this work are to determine the biostratigraphy and paleoenvironmental history at two Ocean Drilling Program (ODP) Leg 139 sites. The Leg 139 locality presents several obstacles to these goals. The sites are probably Quaternary in age because they lie above Brunhes Chron basement. At present, relatively little is known about Quaternary climatic events of the northeast Pacific Ocean (compared to our knowledge of the North Atlantic Ocean, for example) and Quaternary biostratigraphy is inadequately resolved in the region (see "Biostratigraphy of the Northeast Pacific Ocean" section, this chapter). The locality lies in Middle Valley, a spreading center of the Juan de Fuca Ridge, so hydrothermal and thermal alteration play a role in fossil preservation. The valley is thickly sedimented by about a kilometer of turbidites shed from the glaciated margin of British Columbia, and sedimentation rates exceed 190 cm/k.y. (Davis, Mottl, Fisher, et al., 1992, p. 304). The high sedimentation rates produce expanded sequences of Quaternary calcareous fossils in hemipelagic intervals, especially since the locality lies mostly above the regional calcium carbonate compensation depth (CCD) during both glacial and interglacial periods. However, the turbidites also dilute sediments, disrupt trends, and in other ways disturb the sequences.

The effort calls attention to several biostratigraphic and paleoenvironmental issues of wider significance. We do not know at this time if foraminiferal faunas and the water masses they reflect change significantly in the subarctic northeast Pacific during glacial-interglacial cycles or if assemblage change is restricted to the southerly portions of the region. Does the transitional fauna invade the study region during interglacial periods, or is the fauna uniformly subarctic in character throughout the Brunhes? Does the preserved fauna record changes in upwelling, dilution of surface waters, and/or migration of water masses across the study region? Planktonic foraminiferal assemblage zones of the subarctic are poorly defined in the Brunhes. Calcium carbonate and oxygen isotopic stratigraphies suggest that there are six or seven warmings during the Brunhes. Do interglacial planktonic foraminiferal assemblages appear below the present interglacial interval? Do interglacial intervals correspond to carbonate-rich intervals? This exploratory work makes progress toward answering aspects of these questions.

Biostratigraphy of the Northeast Pacific Ocean

Assemblage zones must be used to subdivide the transitional and subarctic North Pacific Ocean during the Pleistocene because there are few evolutionary events among the cold-water planktonic foraminifers during this interval (Lagoe and Thompson, 1988). The simplest type of assemblage zone, the coiling direction zone, has been used to great effect in the transitional water mass and the California Current. Specifically, Pleistocene warm/cold cycles and coiling direction zones have been described using the relative proportions of sinistral and dextral *Nq. pachyderma.*

Placement of the Holocene-Pleistocene boundary in the northeast Pacific Ocean is in question. In the California Borderland, Bandy (1960) recognized a dextral interval in recent sediments underlain by a sinistral interval. The coiling shift between the zones occurred approximately 11,000 yr ago and is widely used to mark the regional Holocene-Pleistocene boundary. More recent work from offshore northern California (Brunner and Ledbetter, 1989; Gardner et al., 1988) shows that a dextral to sinistral couplet lies immediately below the Holocene dextral zone. The base of the dextral interval is dated at about 15,000 yr ago; the sinistral event occurred about 11,500 yr ago (Gardner et al., 1988). The late Holocene is dominated by sinistral *Nq.*

[1] Mottl, M.J., Davis, E.E., Fisher, A.T., and Slack, J.F. (Eds.), 1994. *Proc. ODP, Sci. Results*, 139: College Station, TX (Ocean Drilling Program).

[2] Center for Marine Science, University of Southern Mississippi, Stennis Space Center, MS 39529, U.S.A.

pachyderma that may mark the onset of coastal upwelling in the California Current (Karlin et al., 1992).

The lower and middle Pleistocene is subdivided by the coiling zones of Lagoe and Thompson (1988), who defined nine zones (CD8 to CD16) between 0.6 and 4 Ma. Coiling zones are fairly well defined below 1.2 Ma because coiling shifts are relatively infrequent and boundaries are constrained by a number of evolutionary events. However, coiling zones remain poorly defined between the latest Pleistocene and the CD9/CD10 boundary at about 1.2 Ma.

Coiling dominance has shifted frequently throughout most of the Pleistocene. In general, the lower Pleistocene sequences contain cool and cold assemblages in alternation (Lagoe and Thompson, 1988; Kent et al., 1971), whereas the upper Pleistocene sequences contain a cold assemblage punctuated by a number of short warm intervals. Two extinction events before 0.6 Ma provide some time control for the lower Pleistocene, but no such events occur in the upper Pleistocene (Lagoe and Thompson, 1988), making unique identification of coiling intervals difficult. At present, the geographic extent and number of migrations of dextral *Nq. pachyderma* into the subarctic is unknown, but oxygen isotopic and carbonate stratigraphy suggest that it is reasonable to look for six migrations (Zahn et al., 1991) corresponding to oxygen isotopic stage terminations (Brunner and Ledbetter, 1989; Gardner et al., 1988) 1–2, 5–6, 7–8, 11–12, 13–14, and 15–16.

Pleistocene Paleoenvironmental History

The lower Pleistocene of the North Pacific Ocean was a period of relative warmth dominated by dextral *Neogloboquadrina pachyderma* (Olsson and Goll, 1970; Kent et al., 1971; Ingle, 1973a,b; Lagoe and Thompson, 1988). The climatic warmth extended into the subarctic Pacific Ocean as indicated by the presence of dextral *Nq. pachyderma* in subpolar waters (Kent et al., 1971). Sinistral *Nq. pachyderma* increased abruptly relative to its dextral form after 1.2 Ma, indicating a pronounced cooling throughout the region (Ingle, 1973a; Kent et al., 1971). Thompson (1980) suggests that the dextral morph has been environmentally excluded from the subarctic Pacific Ocean since this major cooling.

The North Pacific has undergone a number of climatic cycles since the cooling 1.2 Ma. Lagoe and Thompson (1988) describe conditions that fluctuate between cold and cool from 1.2 to 0.6 Ma. After 0.6 Ma conditions appear generally cold, but are punctuated by an uncertain number of warm events above the Brunhes-Matuyama boundary (0.73 Ma). Most data come from regions south of the subarctic front. Thompson (1980) identifies six southerly invasions of sinistral *Nq. pachyderma* in the Brunhes Magnetozone in the Japan Trench region that correspond to oxygen isotopic stages 2, 4, 6, 8, 12, and 16, and Kheradyar (1992) shows six or seven northerly invasions of dextral *Nq. pachyderma* into the southernmost Japan Sea.

Carbonate stratigraphy supplies some clues to the number of climatic cycles in the Brunhes Magnetozone. In the subarctic northwestern Pacific Ocean, Kent et al. (1971) observed six carbonate-rich intervals interspersed with barren intervals above the Brunhes-Matuyama boundary in core V20-119. The fossiliferous intervals all contain sinistral *Nq. pachyderma* and were deposited during interglacial periods based on oxygen isotopic ratios (Hays and Shackleton, 1976; Thompson and Shackleton, 1980). The barren intervals apparently correspond to glacial periods in contrast to the general pattern of carbonate preservation in the Pacific Ocean. The preceding results support the suggestion that dextral *Nq. pachyderma* does not penetrate the northwestern subarctic Pacific Ocean even during interglacial periods. The opposite preservation pattern occurs in the subarctic northeast Pacific. Six carbonate-rich intervals were deposited during the Brunhes (Zahn et al., 1991; Karlin et al., 1992; Nayudu, 1964), and they correspond to oxygen isotopic stages 2–3, 6, 8, 12, 14, and 16 (Zahn et al., 1991; Karlin et al., 1992). Coiling curves are not yet available for this suite of cores.

Environmental Setting

Hydrography and Paleohydrography

Surface waters of the subarctic North Pacific Ocean in general are characterized by low temperature and salinity less than 34‰. Subarctic waters are clearly separated from subtropical waters by a strong oceanic front where the 3°C isotherm plunges from 100 m north of the boundary to 1000 m south of the boundary, which lies between 40° and 45°N latitude. Distinctive surface water masses are produced in subarctic waters by the interaction of several processes: winter overturn, which produces a subsurface temperature minimum; dilution from spring and summer meltwaters that spread from the coasts; divergence and upwelling in gyre centers; coastal upwelling; and seasonal ice cover in regions adjacent to the subarctic ocean, such as the Sea of Okhotsk.

Favorite et al. (1976) divide surface waters (upper 300 m) into five domains of distinctive hydrographic characteristics separated by current systems. Leg 139 sites lie at the eastern extreme of the Subarctic Current System where the continent diverts flow to the north as the Alaska Current and to the south as the California Current (Sverdrup et al., 1942), between the Dilute Domain and the Upwelling Domain of the coast (Favorite et al., 1976). Salinities of the Dilute Domain at 50 m and deeper are reduced by spring and summer plumes from the Columbia River, the Strait of Juan de Fuca, Queen Charlotte Sound, and Dixon Entrance and are surrounded by higher salinities brought near the surface by divergence in the surrounding regions. The Upwelling Domain near the study region is active from late spring to early fall. It undergoes seasonal reversal of coastal flow (Davidson and California Currents) and seasonal discharge from the Columbia River. Mean surface temperature in summer is more than 5°C lower, and mean salinities are 0.1‰ to 0.3‰ higher in the Upwelling Domain than in the Dilute Domain. Both domains are distinctively different from the Transition Domain, which lies between them and the Subarctic Boundary. The hydrographic boundaries are reflected in the biogeography of plankton (Bradshaw, 1959). A subarctic fauna lives at the study site and a transitional fauna is found to the south in the Transition Domain.

Conditions during the last glacial maximum 18,000 yr ago were quite different. The Subarctic Boundary lay about 5° south of its present position in the western and central portions of the North Pacific Ocean (Thompson, 1981) and subpolar waters extended down the California coast (Moore et al., 1980). The western and central subarctic were more affected by seasonal ice cover and were similar to the present-day Sea of Okhotsk (Sancetta, 1979). Coastal upwelling offshore from Oregon was greatly reduced and did not return to present-day conditions until 7000 yr ago (Karlin et al., 1992; Lyle et al., 1992). Summer surface-water temperature was 2°C cooler and winter surface-water temperature was 4°C cooler than present-day temperatures (Moore et al., 1980) in the study region.

The CCD depth lies between 2200 and 2700 m at present based on the percentage of carbonate in core-top sediments (Karlin et al., 1992) and near 2700 m based on preservation of subarctic core-top faunas (Coulbourn et al., 1980). In contrast, the CCD migrates to depths between 4400 and 4500 m in the region during Pleistocene glaciations (Karlin et al., 1992). Sites 856 and 857 lie at 2395 and 2418 m water depth, near or above the interglacial upper limit of the CCD. I expect that carbonate fossils will be preserved even during interglacial periods when carbonate preservation in the Pacific Ocean is generally poor (Berger, 1976).

Planktonic Foraminiferal Fauna

Bradshaw (1959) reported that living faunas of planktonic foraminifers have biogeographical distributions that generally follow the outlines of the major water masses (Sverdrup et al., 1942). Middle

Valley (near 48°30′N, 128°45′W) lies near the boundary between the subarctic fauna and the transitional fauna (Bradshaw, 1959), but Bradshaw (1959) was not able to locate the boundary because his samples do not extend into the northeast subarctic. Species found in sediment traps in subarctic waters nearby (50°N, 145°W) include *Turborotalita quinqueloba* (Natland), sinistral and dextral *Nq. pachyderma* (Ehrenberg), *Globigerina bulloides* d'Orbigny, *Orbulina universa* d'Orbigny, *Globigerinita glutinata* (Egger), and *Globorotalia scitula* (Brady) (Reynolds and Thunell, 1985; Reynolds and Thunell, 1986; Sautter and Thunell, 1989). Bradshaw (1959) also reported small *Neogloboquadrina dutertrei* and a form similar to *Globigerinita minuta* (Natland) in his plankton net samples. The transitional fauna of Bradshaw (1959) contains *Globigerina bulloides*, large *Neogloboquadrina dutertrei*, *Turborotalita quinqueloba*, *Orbulina universa*, and *Globigerinoides ruber* and includes a mix of species from neighboring faunas near its boundaries. The central-water assemblage to the south of the transitional fauna is marked by *Globorotalia inflata* and *Globorotalia truncatulinoides* (Bradshaw, 1959).

The distribution of planktonic faunas is mirrored by fossil assemblages in surficial sediment. Coulbourn et al. (1980) found that sinistral *Nq. pachyderma* dominates the fossil assemblage beneath the subarctic fauna of Bradshaw (1959), dextral *Nq. pachyderma* dominates the fossil assemblage beneath the transitional fauna, and *Globorotalia inflata* flags sediments beneath the central-water assemblage. Dissolution on the seafloor modifies planktonic foraminiferal assemblages by removing delicate species. For example, the subarctic fossil fauna becomes enriched in sinistral *Nq. pachyderma* at the expense of solution susceptible species of the subarctic fauna (Sautter and Thunell, 1989; Coulbourn et al., 1980; Berger, 1981).

Geologic Setting of Middle Valley

Sequences at Middle Valley are dominated by turbidite deposition into the rift. The rift valley is a bathymetric low that acts as a depositional trap for turbidites originating on the continental slope of Vancouver Island and Queen Charlotte Sound. Deposition was probably accelerated during low stands of the sea when alpine and continental glaciers added large amounts of debris to the continental slope.

The Leg 139 sites are located near the eastern wall of the valley. Hole 856A is located at the crest (2395 m) of a small hill that stands about 60 m above the surrounding turbidite plain. The southern flank of the hill is associated with several sulfide mounds. The hole terminates at a mafic sill intruded at 115 mbsf within the sediment pile, which was somewhat altered during intrusion and cooling of the sill. Site 856 lies on crust that could be as old as 320,000 yr based on its distance from the east edge of the Brunhes magnetic chron.

Site 857 sits on a block that has been uplifted a few tens of meters above and tilted eastward from the turbidite plain of the valley axis. Sediments at this locality are thick, consisting of 470 m of turbidites and an additional 457 m of interbedded sills and sediments. Heat flow is high at the site, which lies between a large hydrothermal vent field and the presumed fluid recharge area at the eastern faulted rim of the valley. Age of basement is about 250,000 yr old based on spreading rates.

METHODS

The sequences at Middle Valley consist mostly of silt- and sand-based turbidites interspersed with unsorted silty clays and clayey silts which could be turbiditic or hemipelagic. Most foraminiferal samples were selected from the unsorted silt and clay units to minimize sampling of sorted and displaced faunas. Core photos were used to verify the lithology of each sample because most samples were not taken personally by the author. All samples span 2 to 3 cm of depth in core, and so potentially average together fine-scale depositional units characteristic of silt-based turbidites (Stow and Piper, 1984; Brunner and Ledbetter, 1987, 1989).

Samples were prepared for planktonic foraminifers using conventional micropaleontologic techniques. Samples were oven-dried at 50°C, weighed, soaked in a 1% Calgon solution for 1 hr, and washed in a sieve with 63-µm openings. Samples washed on board the *Resolution*, however, were not weighed. The sand-size residue was oven-dried at 50°C and inspected microscopically to identify and rank qualitative abundance of the constituents. The sand content (% by weight) of all weighed samples was calculated.

The depth of the Holocene-Pleistocene boundary (Bandy, 1960) was determined in Holes 855A, 855C, 856A, 856B, 857A, 857B, 857C, 858A, 858C, and 858D using the coiling ratio of *Nq. pachyderma*. A minimum of 30 specimens was inspected for coiling direction to calculate the relative frequency of sinistral forms (number of sinistral forms/[number of sinistral + number of dextral forms]). The minimum of 30 specimens has a probable error greater than 15% for relative frequencies less than 40%. (Krumbein and Pettijohn, 1938, fig. 245). The sensitivity is sufficient for detection of potential interglacial samples that have sinistral frequencies less than 90%.

Holes 856A, 857A, and 857C were selected for assessment of Pleistocene planktonic foraminiferal biostratigraphy and paleoenvironment. Samples selected from Hole 857C (115.46 to 389.7 mbsf) underlie those at 857A (0 to 108.38 mbsf). The three holes were chosen because foraminifers are preserved to great depth and two of the holes (856A and 857A) were hydraulically piston-cored ensuring minimal coring disturbance. A census of species was made in all 103 samples in which a minimum of 300 planktonic foraminifers was found. The samples were split using a modified Otto microsplitter when necessary. The number of benthic foraminifers was also noted during the census. Several terms were calculated from these data including (1) the benthic foraminiferal frequency (100 · number of benthic foraminifers/[number of benthic + number of planktonic foraminifers]), (2) the planktonic foraminiferal number (number of planktonic foraminifers/[fraction of sample counted] [dry sediment weight]), (3) the coiling ratio of *Nq. pachyderma* (100 · sinistral forms/[sinistral + dextral forms]), and (4) the relative frequency of common planktonic foraminiferal species (see "Taxonomic Notes" section, this chapter).

Cluster analysis was used to group together samples with the most similar species composition (Q-mode). The analysis agglomerated unweighted samples with the simple Euclidean distance coefficient using the average linkage (within group) method. Several other methods of agglomeration were tried and produced similar basic groupings indicating that the basic groupings were fairly stable. Several samples, however, were joined to different groups depending on the agglomeration method. These samples apparently lie at the boundaries of the clusters and are intermediate in their species composition. The clustering effort succeeds in defining basic groupings and is not intended to optimally group every sample. The validity of the sample clusters, which are based on similarity of species composition, was corroborated by calculating Pearson correlation coefficients between pairs of species to demonstrate the strength of their associations.

RESULTS

Lithology

Many samples contain at least some sediment that is turbiditic in origin. Sample intervals were examined from the core photos to determine lithology (Tables 1 and 2). Two samples were taken from the disturbed soft mud or sand between hard "biscuits" formed during drilling of semi-indurated sediments. These samples are likely contaminated with material slumped down the hole. Two samples were taken in well-sorted silt layers and are wholly turbiditic. Many samples (30) contain a thin layer (of millimeters) or blebs of well-sorted silt amid mostly muddy material, so the samples contain at least some turbiditic material which may be mixed with hemipelagic sediment. Some samples (43) are from the muddy tops of fining upward sequences. The muds may be hemipelagic, turbiditic, or a bioturbated

Table 1. Constituents of the sand-size fraction, Hole 856A.

Core, section, interval (cm)	Depth (mbsf)	Sand	Fno	B/P	Coil	Lith	Constituents of the sand-size fraction
139-856A-							
1H-1, 0–1	0.00			57	85	Mud	Clay lumps, radiolarians, diatoms, foraminifers
1H-1, 91–93	0.91	1.5	8160	2	97	Mud	Forams, pyrite
1H-2, 48–50	1.98	1.8	4998	2	97	Mud	Forams, pyrite
2H-2, 90–92	5.10	0.3	167	29	99	Mud	Forams, pyrite, radiolarians
2H-3, 90–92	6.60	0.1	22	7	98	Top fus	Pyrite, mineral grains, forams
2H-4, 101–103	8.21	0.4	339	18	99	Mud	Forams, pyrite, mineral grains
2H-5, 86–88	9.56	0.3	131	48	97	Top fus	Pyrite, forams
2H-6, 86–88	11.06	0.6	1133	5	98	Top fus	Forams, pyrite, mineral grains, radiolarians
2H-7, 56–58	12.26	0.8	1928	1	98	Mud	Forams, pyrite, mineral grains
3H-3, 72–74	15.92	0.2	185	9	100	Top fus	Forams, pyrite
3H-4, 91–93	17.61	0.3	227	9	87	Mud, fault	Pyrite, forams
3H-4, 117–119	17.87	0.7	610	9	44	Mud	Forams, pyrite
3H-5, 74–76	18.94	0.2	232	27	28	Mud	Forams, pyrite, test fragments very abundant
3H-5, 78–80	18.98	0.3	414	13	29	Mud	Pyrite, forams
3H-5, 96–98	19.16	0.5	381	12	12	Mud	Forams, pyrite, silt lumps
3H-5, 108–110	19.28	2.0			17	Mud	Mineral grains, forams, pyrite
3H-5, 130–132	19.50	0.6	827	6	29	Mud	Forams, pyrite
3H-6, 92–94	20.62	4.3	11811	7	97	Mud	Forams, overgrowths, cement, horns
3H-7, 39–41	21.59	0.6	0			Dark mud	Mineral grains, pyrite, forams, overgrowths, cemented mineral grains
4H-1, 82–84	22.52	0.8	389	30	96	Top fus	Forams, pyrite, strong overgrowths
4H-2, 81–83	24.01	1.2	760	6	97	Top fus	Forams, pyrite, strong overgrowths
4H-3, 122–124	25.92	1.4	1541	2	99	Top fus	Forams, pyrite, strong overgrowths
4H-4, 88–90	27.08	0.9	29	20	91	Top fus	Cemented mineral grains, rare forams, overgrowths
4H-5, 96–98	28.66	3.4	3947	3	97	Top fus	Forams, overgrowths
4H-6, 108–110	30.23	13.0	1526	9	99	Silty blebs	Mineral grains, rare forams, overgrowths, cement
4H-7, 62–64	31.32	0.5	446	3	99	Mud	Forams, mineral grains, overgrowths, cemented grains on forams
5H-1, 19–21	31.39	3.4	3999	2	100	Top fus	Forams, mineral grains, overgrowths, cemented grains on forams
5H-2, 6–8	31.64	1.3	265	62	100	Top fus	Mineral grains, forams, overgrowths
5H-3, 135–137	34.43	9.9	339	44	100	Top fus	Mineral grains, forams, overgrowths, cemented silt lumps
5H-4, 88–90	35.46	3.1	3952	2	100	Top fus	Forams, pyrite, overgrowths
5H-5, 133–135	37.41	2.0	431	39	99	Top fus	Mineral grains, rare forams, some with overgrowths
5H-6, 90–92	38.48	0.7				Top fus	Mineral grains, forams, pyrite, overgrowths, mixed preservation
5H-7, 88–90	39.96	3.5	475	58	100	Silty	Mineral grains, pyrite, forams, overgrowths
6H-1, 68–70	41.38	2.5	448	54	99	Silty	Mineral grains, forams, pyrite, overgrowths
6H-2, 123–125	43.43	0.2	17	75	100	Top fus	Cemented silt lumps, forams, pyrite, overgrowths
6H-3, 127–129	44.97	2.4	3872	6	100	Top fus	Forams, pyrite, overgrowths
6H-4, 138–140	46.58	4.7	0			Top fus	Mineral grains
6H-5, 73–75	47.43	3.5	0			Silty	Mineral grains
6H-6, 46–48	48.66	0.2	243	53	99	Top fus	Mineral grains, forams, overgrowths
6H-6, 112–114	49.32	1.4	108	9	100	Top fus	Mineral grains, forams, overgrowths
7H-1, 48–50	50.68	4.7	273	38	100	Silty	Mineral grains, forams, overgrowths
7H-2, 12–14	51.82	4.0	1049	13	100	Top fus	Forams, mineral grains, pyrite, overgrowths
7H-2, 101–103	52.71	5.5	0			Silty	Mineral grains
7H-4, 64–66	55.34	27.0	0			Silty	Mineral grains
7H-4, 94–96	55.64	20.3	0			Silty	Mineral grains
7H-5, 46–48	56.66	16.9	0			Silty	Mineral grains
7H-6, 39–41	58.09	4.8	0			Silty	Mineral grains
7H-7, 23–25	59.43	3.4	0			Silty	Mineral grains
8H-1, 87–90	60.57	0.0	0			Top fus	Pyrite, sulfate(?) crystals, agglut forams
8H-2, 119–121	62.39	9.2	0			Silty	Mineral grains, pyrite
8H-3, 120–123	63.90	0.1	0			Mud	Mineral grains, agglut forams, sulfate(?) crystals
8H-4, 112–115	65.32	0.4	0			Mud	Mineral grains
8H-5, 98–101	66.68	2.7	0			Mud	Mineral grains, rare forams with overgrowths
8H-6, 94–98	68.14	1.8	0			Mud	Mineral grains, pyrite, forams, cemented mineral lumps
9H-1, 127–129	70.47	0.1	0			Mud	Pyrite, agglut forams, sulfate(?) crystals
9H-2, 122–124	71.92	0.5	0			Top fus	Mineral grains, pyrite, agglut forams
9H-3, 90–92	73.10	0.4	0			Top fus	Agglut forams, pyrite, cemented mineral grains
9H-4, 97–99	74.67	1.5	0			Top fus	Agglut forams, mineral grains, pyrite
9H-5, 127–129	76.47	0.6	0			Top fus	Cemented silt lumps, pyrite, rare recrystallized benthics, agglut forams
9H-6, 46–48	77.16	0.1	6	0	100	Mud	Pyrite, mineral grains, forams (white)
10X-1, 20–23	78.90	0.7	0			Top fus	Cemented silt lumps, pyrite, sulfate(?) crystals
10X-2, 85–88	81.05	0.7	0			Top fus	Mineral grains, cemented silt lumps
11X-1, 12–14	86.32	1.5	0			Top fus	Silt lumps, magnetite, pyrite, lumps >500µm
11X-2, 8–10	87.78	17.5	0			Top fus	Silt lumps, some lumps >500µm
11X-2, 10–12	87.80	19.9	0			Top fus	Silt lumps, pyrite, lumps >500µm
12X-1, 33–35	96.03	1.8				Top fus	Mineral grain lumps, pyrite, brown recrystallized forams
12X-2, 32–34	97.52	9.9				Drill sand	Pyrite, mineral grains, brown forams
13X-1, 65–67	105.95	0.7	0			Mud	Silt lumps, pyrite, mineral grains
13X-2, 57–60	107.37	0.3	0			Top fus	Silt lumps
13X-3, 4–6	108.34	25.9	0			Mud	Cemented silt lumps, pyrite, mineral grains, lumps >500µm
13X-4, 87–89	110.67	15.6	0			Mud	Mineral grains, pyrite, lumps >500µm
13X-5, 18–20	111.48	23.6	0			Drill mud	Cemented silt lumps, pyrite, mineral grains, lumps >500µm

Notes: mbsf = meters below seafloor; Sand = percent greater than 63 micrometer fraction by weight; Fno = foraminiferal number (test/g); B/P = relative frequency of benthic foraminifers to total number of foraminifers; Coil = relative frequency of sinistral *Nq. pachyderma* to total number of *Nq. pachyderma*; Lith = lithology; Mud = unconsolidated silty clay or clayey silt; Top fus = muddy top of a fining upward sequence; Silty = sample contains silty blebs, wisps, or layers; Claystone = consolidated silty clay or clayey silt; Constituents of the sand size fraction are ranked in order of greatest abundance; forams = planktonic and/or benthic foraminifers.

Table 2. Constituents of the sand-size fraction, Holes 857A and 857C.

Core, section, interval (cm)	Depth (mbsf)	Sand	Fno	B/P	Coil	Lith	Constituents of the sand-size fraction
139-857A-							
1H-1, 0–1	1.90			8	85	Mud	Forams
1H-1, 79–81	2.69	1.8	1287	2	97	Silty	Forams, mineral grains, pyrite
1H-2, 125–129	4.65	1.0	1606	2	99	Silty	Forams, mineral grains, pyrite
1H-3, 10–13	5.00	1.8	5864	1	100	Mud	Forams
1H-3, 23–27	5.13	1.7				Silty	Forams, pyrite
1H-4, 72–76	7.12	0.4	1	13	100	Silty	Mineral grains, pyrite
1H-5, 89–91	8.79	1.3	5331	1	100	Mud	Forams, pyrite
1H-6, 36–38	9.76	1.0	2805	4	99	Silty	Forams, pyrite
2H-1, 45–48	11.85			7	100	Mud	Forams, pyrite
2H-1, 97–99	12.37	1.2	2784	4	99	Mud	Forams, pyrite
2H-1, 105–107	12.45			9	99	Silty	Forams, pyrite
2H-2, 20–22	13.10			2	100	Top fus	Forams, pyrite
2H-2, 96–98	13.86	1.4	2999	4	100	Top fus	Forams, pyrite
2H-2, 129–131	14.19			9	100	Mud	Forams, pyrite
2H-3, 98–100	15.38	0.1	356	5	98	Mud	Forams, pyrite
2H-3, 129–131	15.69			21	100	Mud	Forams, pyrite
2H-4, 12–14	16.02			16	99	Mud	Pyrite tubes, forams, mineral grains
2H-4, 98–100	16.88	0.3	526	14	99	Top fus	Forams, pyrite
2H-4, 127–129	17.17			22	99	Mud	Forams, pyrite
2H-5, 7–9	17.47	0.6	444	10	99	Mud	Pyrite tubes, forams
2H-5, 22–24	17.62			7	100	Mud	Forams, pyrite
2H-6, 9–11	18.99			11	98	Top fus	Forams, pyrite, some yellow tests
2H-6, 93–95	19.83	0.3				Mud	Silt lumps, forams, pyrite
2H-7, 26–28	20.66	0.4	715	11	98	Top fus	Pyrite, forams
4H-1, 124–126	23.14	1.5				Silty	Mineral grains, pyrite, forams
4H-2, 105–107	24.45				100	Mud	Pyrite, forams, sponge
4H-2, 118–122	24.58	1.8	0			Silty	Mineral grains, pyrite
4H-3, 64–66	25.54	0.2	27	38	98	Top fus	Pyrite, forams, mineral grains
4H-3, 100–103	25.90	3.4				Silt layer	Mineral grains, pyrite, forams, rad
4H-3, 115–117	26.05				97	Mud	Mineral grains, silt lumps, forams
4H-3, 125–127	26.15	0.6	281	19	99	Mud	Forams, radiolarians, pyrite
4H-4, 12–14	26.52	0.7	70	55	90	Mud	Pyrite, forams, diatoms, radiolarians
4H-4, 30–32	26.70	1.2	23	47	96	Mud	Pyrite, mica, forams, radiolarians
4H-4, 38–40	26.78	0.6			90	Mud	Forams, pyrite, radiolarians, diatoms
4H-4, 49–51	26.89			26	78	Top fus	Forams, silt lumps, pyrite
4H-4, 59–61	26.99	0.1			100	Mud	Radiolarians, forams, pyrite
4H-4, 70–74	27.10	0.1	10	73	96	Top fus	Pyrite, forams
4H-5, 40–44	28.30	0.2	256	11	99	Mud	Forams, pyrite
4H-5, 127–129	29.17				100	Silty	Forams, pyrite, mineral grains
4H-7, 43–47	31.33	0.4	638	11	95	Mud	Forams, pyrite
5H-2, 13–17	33.03	0.1	40	18	98	Mud	Pyrite, mineral grains, forams
5H-2, 38–42	33.28	2.4	0			Silt layer	Mineral grains
5H-3, 48–52	34.88	0.6	0			Silty	Mineral grains, pyrite
5H-4, 9–13	35.99			39	90	Silty	Forams, rads, pyrite
5H-4, 43–45	36.33	1.5			67	Mud	Mineral grains, pyrite, radiolarians, forams
5H-4, 57–61	36.47	3.1	260	25	72	Silty	Mineral grains, forams, radiolarians
5H-4, 70–72	36.60	0.4	56	16	71	Mud	Radiolarians, diatoms, pyrite, forams
5H-4, 130–132	37.20	0.9	212	25	78	Mud	Radiolarians, forams, diatoms, pyrite
5H-5, 105–107	38.45	0.5	269	18	10	Mud	Radiolarians, pyrite, forams
5H-5, 118–120	38.58	0.5	0			Mud	Mica, pyrite, diatoms, radiolarians, forams
5H-5, 126–130	38.66	2.2			20	Silty	Mineral grains, radiolarians, forams
5H-5, 140–142	38.80	0.7	890	8	8	Mud	Radiolarians, pyrite, forams, mica
5H-6, 126–130	40.16	2.6	0		81	Silty	Mineral grains
5H-7, 18–22	40.58	1.8			100	Silty	Mineral grains, pyrite, forams
6H-1, 59–63	41.49	1.0	3142	1	99	Mud	Forams, pyrite
6H-2, 76–80	43.16	1.2	807	1	97	Mud	Forams, pyrite
6H-6, 84–86	49.24	0.1				Mud	Forams
7H-3, 37–39	52.59	0.4	897	6	99	Mud	Forams, pyrite, mineral grains
7H-4, 85–89	54.47	2.2	5688	1	97	Mud	Forams
7H-5, 75–79	55.52	0.4	1247	3	96	Top fus	Forams
7H-6, 121–125	56.59	0.3	980	4	100	Mud	Forams, pyrite
7H-7, 28–32	57.35	0.0	7	6	98	Mud	Pyrite tubes, forams
8H-1, 119–123	61.09	4.1	1602	2	99	Mud	Mineral grains, forams
8H-2, 21–25	61.61	0.5	1061	3	100	Mud	Forams, pyrite
8H-3, 54–58	63.44	1.4	1468	3	99	Silty	Mineral grains, forams
8H-4, 43–47	64.83	0.6	2027	4	99	Mud	Forams, pyrite
8H-5, 40–44	66.30	0.3	277	8	100	Mud	Forams, pyrite
8H-5, 114–118	67.04			2	100	Mud	Forams
8H-6, 52–56	67.92	0.2	766	2	99	Mud	Forams, pyrite
8H-7, 22–26	69.12	0.2	8	29	100	Mud	Pyrite tubes, forams
9H-1, 89–91	70.29	2.0				Mud	Pyrite, rare forams
9H-2, 90–92	71.80	1.2				Mud	Pyrite, forams, mineral grains
9H-3, 74–80	73.14	0.2	717	2	100	Mud	Forams, pyrite
9H-4, 60–63	74.50	1.4	348	5	100	Mud	Pyrite, forams, mineral grains
9H-5, 79–84	76.19			1	98	Mud	Forams, pyrite
10H-1, 124–27	80.14	0.1	350	3	99	Mud	Forams, pyrite
10H-2, 12–14	80.52			5	99	Mud	Forams, silt lumps
10H-4, 99–01	84.39	0.1	94	2	100	Mud	Forams, pyrite
10H-5, 32–34	85.22		0			Mud	Silt lumps, pyrite
10H-6, 12–14	86.52		0			Silty	Mineral grains
13X-1, 9–11	101.59	0.4	0			Claystone	Sulfate(?) crystals, pyrite, mineral grains
13X-2, 63–67	103.63	0.8				Claystone	Forams, cemented silt lumps, pyrite, mineral grains
13X-2, 68–72	103.68		0			Claystone	Cemented mineral grains
13X-3, 90–92	105.40	3.1				Top fus	Mineral grains, forams
13X-4, 95–97	106.95	0.8	0			Claystone	Cemented silt lumps

Table 2 (continued).

Core, section, interval (cm)	Depth (mbsf)	Sand	Fno	B/P	Coil	Lith	Constituents of the sand-size fraction
13X-5, 6–8	107.56	1.8				Claystone	Silt lumps, forams
13X-5, 88–90	108.38	4.9	0			Silty	Mineral grains
139-857C-							
9R-1, 96–98	115.46	0.3	0			Claystone	Mineral grains, sulfate(?) crystals, orange pollen
10R-1, 33–35	124.28					Claystone	Pyrite tubes, orange forams
11R-1, 52–54	134.32					Claystone	Mineral grains, cemented silt lumps, pyrite, white forams
12R-1, 91–94	144.41	0.0				Claystone	Cemented silt lumps, pyrite, sulfate(?) crystals, white forams
12R-2, 31–33	145.31					Claystone	Cemented sand lumps, sulfate(?) crystals, pyrite, recrystallized forams
13R-1, 48–50	153.58	0.0				Claystone	Cemented silt lumps, pyrite, recrystallized forams, a few are brownish
14R-1, 35–39	163.15	0.5	0			Claystone	Cemented silt lumps
14R-2, 68–70	164.98	0.6				Claystone	Mineral grains, cemented silt lumps some >500µm, light brown recrystal. forams
15R-1, 32–34	172.82	0.1	0			Claystone	Mineral grains, sulfate(?) crystals, pyrite
15R-2, 40–42	174.40	0.1	0			Claystone	Sulfate(?) crystals
15R-3, 12–14	175.62	0.2				Claystone	Calcite crystals, light brown forams with overgrowths, some lumps >500µm
15R-4, 10–14	177.10	45.3	0			Claystone	Cemented silt lumps, pyrite, some lumps >500µm
15R-5, 17–20	178.67	19.4	0			Claystone	Cemented silt lumps, some lumps >500µm
16R-1, 7–9	182.27	0.5	0			Claystone	Cemented silt lumps, pyrite
17R-1, 49–51	192.39	0.2	0			Claystone	Cemented silt grains, pyrite, mineral grains, some lumps >500µm
18R-1, 49–51	202.09	28.1	0			Claystone	Cemented silt lumps, pyrite, some lumps >500µm
19R-1, 45–47	211.75	36.0	0			Claystone	Cemented silt lumps, some lumps >500µm

Notes: mbsf = meters below seafloor; Sand = percent greater than 63 micrometer fraction by weight; Fno = foraminiferal number (test/g); B/P = relative frequency of benthic foraminifers to total number of foraminifers; Coil = relative frequency of sinistral *Nq. pachyderma* to total number of *Nq. pachyderma*; Lith = lithology; Mud = unconsolidated silty clay or clayey silt; Top fus = muddy top of a fining upward sequence; Silty = sample contains silty blebs, wisps, or layers; Claystone = consolidated silty clay or clayey silt; Constituents of the sand size fraction are ranked in order of greatest abundance; forams = planktonic and/or benthic foraminifers; rads = radiolarians.

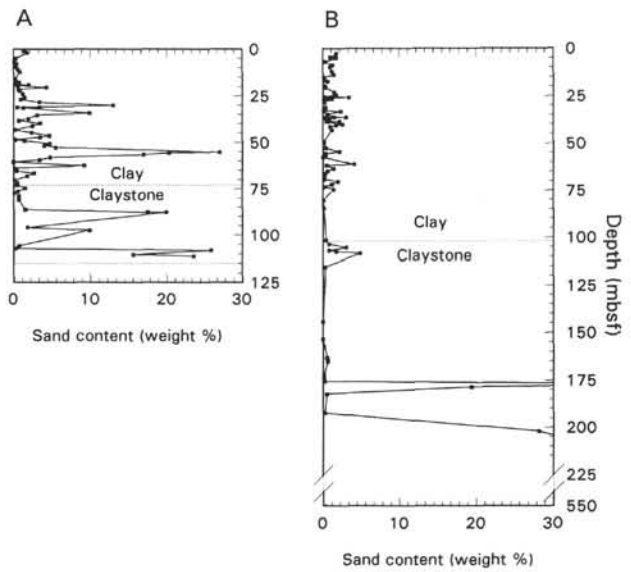

Figure 1. Sand contents of samples in (**A**) Hole 856A and (**B**) Holes 857A and 857C measured by the percent by weight of particles greater than 63 µm in diameter. The depths of the first semilithified samples are marked by the upper dotted lines. The top of a basaltic sill at the base of Hole 856A is marked by the second dotted line in A. Hole 857A terminated in sediment interlayed with sills.

Table 3. Statistics on constituents of the sand-size fraction.

Statistical terms	Hole 856A			Holes 857A and 857C		
	Sand	Fno	B/P	Sand	Fno	B/P
Median	1.4	446	9	0.6	638	7
Mean	4.2	1505	21	2.6	1145	12
Number of samples	70	37	38	77	43	58

Notes: Sand = percent by weight >63 µm; Fno = planktonic foraminiferal number (tests/gm of sediment); BP = frequency of benthic foraminifers (benthic tests/total foraminiferal tests).

mixture of grains from both depositional regimes. Some samples (22) were semi-indurated claystone in which sediment texture and structure were difficult to determine based on the core photos. Presence of sand-size aluminosilicate mineral grains suggests that 10 of the claystones contain some turbiditic sediment. Some samples (77) were taken from muddy units with no recognizable structure. These samples have a higher probability of being hemipelagic than do samples from the other types of units.

The constituents in the sand-size fraction of the muds and tops of fining upward sequences (Tables 1 and 2) support the contention that many of these samples could be hemipelagic rather than turbiditic in depositional origin. Most samples from muds (52 of 77 samples) are composed of pelagic grains such as authigenic pyrite, radiolarians, and foraminifers, whereas 25 samples contain various amounts of aluminosilicate mineral grains. Almost one third of the samples from the tops of fining upward sequences (15 of 43) consist of pelagic constituents, usually foraminifers with various amounts of authigenic pyrite, and the remainder contain either sand-size mineral grains or cemented silt lumps. The lithologic results make clear that the micropaleontologic data at Sites 856 and 857 must be interpreted with caution. Only about 40% of the samples in the data set are likely to be hemipelagic (67 of 176), and the remainder are either turbiditic or the style of deposition is obscured by postdepositional effects. Turbiditic samples will be flagged on graphs used for biostratigraphy and paleoenvironmental analysis.

Comparison of the constituents of the sand-size fractions of Hole 856A and Hole 857A reveal distinctive trends (Table 3). The sand content (percent by weight) at Hole 856A is significantly greater than the sand content at Holes 857A and 857C. More significance is given to the comparison of medians because the distributions are not normal. At Site 857 (Table 2; Fig. 1), only four samples have sand contents above 5%, and these are semilithified sediments from the base of Hole 857A and from underlying depths at Hole 857C. In contrast, Hole 856A has 13 samples coarser than 5% (Table 1; Fig. 1): five of these are slightly indurated sediments from the deepest three cores, six are dominated by aluminosilicate mineral sands, and one is filled with pyrite. Most samples that contain 1% to 5% sand at either site contain abundant mineral grains, pyrite, or sometimes planktonic foraminifers, but some samples below 18.5 mbsf at Hole 856A are coarse because grains have been cemented together into sand-size lumps.

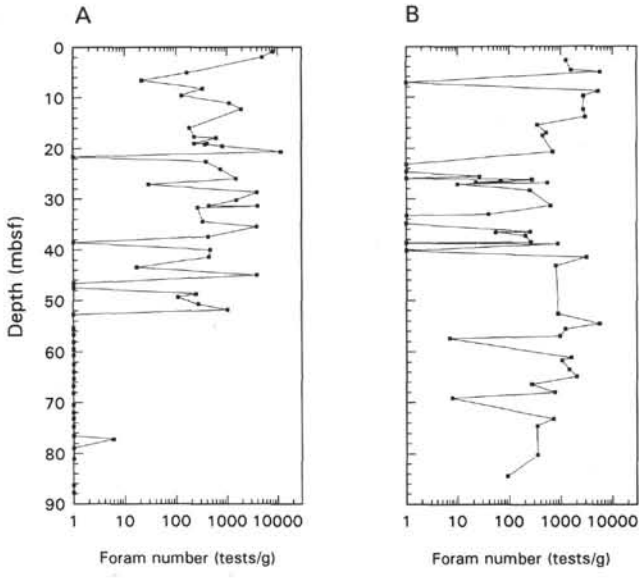

Figure 2. Foraminiferal numbers of samples in (**A**) Hole 856A and (**B**) Hole 857A measured by the number of planktonic foraminiferal tests per gram of dry bulk sediment.

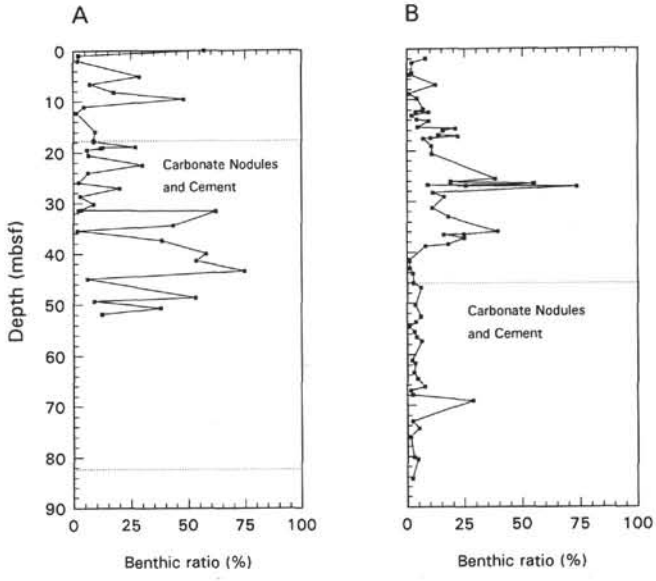

Figure 3. Benthic ratios of samples in (**A**) Holes 856A and 857A (**B**) measured by the frequency of benthic foraminifers relative to benthic plus planktonic foraminifers. Intervals where carbonate nodules and cement occur are marked between dotted lines in **A** and below the dotted line in **B.**

Fossil Abundance

Planktonic foraminifers are abundant at Hole 856A in most sections above 52 mbsf, but occur rarely and sporadically below this depth. They are abundant at Holes 857A and 857C above 85 mbsf, but are rare and sporadic from 85 mbsf to 221 mbsf, absent to 332 mbsf, sporadic to 390 mbsf, and barren to the bottom of the hole at 558 mbsf. Planktonic foraminiferal number (tests/g) was determined in samples above 52 and 85 mbsf, respectively, in Holes 856A and 857A (Tables 1, 2, and 3; Fig. 2). The median of Hole 857A is larger than that of 856A, but Hole 856A has the two highest planktonic foraminiferal numbers. At both holes, samples with less than 1% sand content also have foraminiferal numbers below 2000 test/g.

The frequency of benthic foraminifers (benthic foraminiferal tests/[planktonic + benthic foraminiferal tests]) was determined in samples above 52 and 85 mbsf, respectively, in Holes 856A and 857A (Tables 1, 2, and 3; Fig. 3). Benthic foraminiferal frequencies have similar medians (9 and 7) at the two holes (Table 3), but the distributions are different. Hole 856A has more samples with high or low frequencies and Hole 857A has more samples with intermediate frequencies. All samples with large foraminiferal numbers (>2000 tests/g) have relatively low benthic test frequencies (<6%), and all samples with a benthic test frequency >15% have very low foraminiferal numbers (<500 test/g).

Fossil Preservation

The preservation state of foraminifers at Holes 856A, 857A, and 857C reflects effects of thermal and hydrothermal alteration. Foraminifers in the fossil-rich upper sequence from 19 to 52 mbsf at Hole 856A bear calcite overgrowths. The overgrowths frost many specimens and have grown to distinct protuberances (wart- and horn-shaped) on specimens from 22 to 26 mbsf. Foraminifers from deep in the sequences appear recrystallized and are a distinctive light brown color. Such specimens occur below 96 mbsf at Hole 856A and below 153 mbsf at Hole 857C. The preservation state is best exemplified in Sample 857C-40R-CC, which bears abundant planktonic foraminifers. All tests are a distinct brown color rather than white, and many tests are deformed in shape by stretching or flattening. The brown color may be produced by maturation of glycosaminoglycan membranes that lie between layers of calcite crystals in planktonic foraminiferal tests (Langer, 1992).

Biostratigraphy

Top of Holocene and Holocene-Pleistocene Boundary

The core tops were sampled from the 11 holes considered here. Samples from the surface (zone of bioturbation) were recognized based on the presence of a characteristic assemblage of agglutinated foraminifers (Table 4). The assemblage includes *Ammodiscus*, *Hormosina*, *Saccammina*, several types of tube fragments, *Ammodiscus*, *Haplophragmoides*, *Cribrostomoides*, and sporadic occurrences of other genera. None of these taxa was found below the topmost sample at any hole in this study. Delicate agglutinated taxa may be restricted to the surface because cements dissolve after burial (Sidner and McKee, 1976). Nine of the eleven core tops bear the agglutinated assemblage and are, therefore, from the surface layer (Holes 885A, 855C, 856A, 856B, 857B, 857C, 858A, 858C, and 858D). Two samples lack the agglutinated foraminifers. The core top from Hole 857A contains abundant benthic and planktonic foraminifers, but no agglutinated taxa. The core top cannot be from the surface. The core top from Hole 858B is barren of all microfossils and contains only hydrothermal anhydrite. Its relation to the surface is uncertain.

The age of core top samples was examined using the coiling ratio of *Nq. pachyderma* and verified using abundance of siliceous microfossils (Table 5). Dextral forms dominate Holocene and latest Pleistocene age sediment (after 14,000 yr) and sinistral forms dominate late Pleistocene sediments of the North Pacific Ocean (Bandy, 1960; Brunner and Ledbetter, 1987; Gardner et al., 1988). The age based on coiling ratio was further corroborated using the abundance of radiolarians and diatoms which dominate biogenic sediment of the Holocene northeast Pacific Ocean after 7000 yr ago (Duncan et al., 1970; Karlin et al., 1992). All samples that bear the surface marker assemblage of agglutinated foraminifers are also Holocene in age (Table 4) based on the coiling ratio of *Nq. pachyderma* and abundance of siliceous microfossils except the core top from Hole 856B. The top of Hole 856B contains only rare fragments of agglutinated taxa, and age indicators suggest a Pleistocene age. The sample is dominated by sinistral *Nq. pachyderma* and has only rare, poorly preserved radio-

Table 4. Estimated depths of Holocene-Pleistocene boundary.

Hole	Depth of deepest Holocene sample (mbsf)	Depth of shallowest Pleistocene sample (mbsf)	Depth of H/P boundary (mbsf)	Stratigraphic error (± m)	Presence of radiolarians, diatoms, and agglutinated taxa in core-top samples
855A	1.01	2.49	1.75	0.74	Radiolarians, diatoms, *Saccammima* sp. A, *Ammodiscus*, *Saccammina* sp. B, *Haplophragmoides*, *Reophax*, orange tubes, thick-wall tubes
855C	0.90	2.06	1.48	0.58	Radiolarians, diatoms, *Reophax* sp. B, rare agglutinated tubes, thick-wall tubes
856A	0.00	0.92	0.46	0.46	Radiolarians, diatoms, flattened *Haplophragmoides*, *Ammodiscus*, *Reophax* sp. B, *Saccammina* sp. A, *Reophax*, *Eggerella*, orange tubes, thick-wall tubes
856B		0.00			Rust stained radiolarians, rare fragments of *Ammodiscus*, *Reophax*, *Saccammina* sp. A, flattened *Haplophragmoides*, orange tube, thick-wall tube
857A	1.91(?)	2.70(?)	2.31(?)	0.40	Very rare radiolarians, no agglutinated specimens found
857B	0.81	1.68	1.25	0.43	Radiolarians, diatoms, organic material, *Saccammina* sp. A, *Reophax* sp. B
857C	0.62	1.67	1.15	0.53	Radiolarians, diatoms, organic material, flattened *Haplophragmoides*, *Reophax* sp. A, *Reophax* sp. B, *Ammodiscus* fragment, *Saccammina* fragment, other rare agglutinated genera, orange tubes, thick-wall tubes
858A	0.00	0.49	0.25	0.25	Radiolarians, diatoms, clay lumps, *Reophax*, *Eggerella*, *Ammodiscus*, orange tubes
858B	Barren	0.90	0.45(?)	0.45	Anhydrite
858C	0.00	1.21	0.61	0.61	Radiolarians, diatoms, clay lumps, *Ammodiscus*, *Saccammina* sp. A, *Reophax*, *Eggerella*, *Cribrostomoides*, orange tubes, other tubes
858D	Barren	2.11	1.06(?)	1.06	Radiolarians, diatoms, clay lumps, *Ammodiscus*, *Saccammina* sp. A, *Reophax*, *Cribrostomoides*, *Haplophragmoides*, orange tubes, other tubes

larians. The apparent unconformity at the top of this hole is supported by the paleomagnetic data.

Two remaining topmost samples have special problems. One top sample (857A) has dextral *Nq. pachyderma* and is Holocene or latest Pleistocene in age (younger than 14,000 yr), but contains few radiolarians and no agglutinated foraminifers, indicating that it probably is older than 7000 yr (Karlin et al., 1992). This sample is probably from the subsurface as a result of overpenetration during initial coring. The sample was reassigned to a depth of 1.91 mbsf based on operational criteria (see "Operations" section, "Site 857" chapter, Davis, Mottl, and Fisher, 1992). The age of the last core top (858B) is uncertain because the surficial hydrothermal sediment is barren of planktonic foraminifers.

The Holocene-Pleistocene boundary was tentatively placed in 8 of 11 holes based on the coiling ratio of sinistral and dextral *Nq. pachyderma* (Table 4). I have assumed that the base of the coiling shift to dextral *Nq. pachyderma* at the tops of the holes occurred 11,000 yr ago (Bandy, 1960) at the regional Holocene-Pleistocene boundary. The boundary, however, cannot be placed at three holes because Holocene-age sediments are absent. Pleistocene-age sediments outcrop at the surface of Hole 856B. Pleistocene fossils occur below samples barren of planktonic foraminifers at Holes 858B and 858D.

Pre-Holocene Interglacial Assemblages

The coiling ratio of *Nq. pachyderma* was examined in the pre-Holocene sequences of Holes 856A and 857A (Fig. 4; Tables 1 and 2). Most of the 103 foraminifer-rich samples at both holes have frequencies of sinistral *Nq. pachyderma* greater than 95%. An unusual sample of abundant recrystallized planktonic foraminifers from 375 mbsf in Hole 857C has a similarly high ratio of sinistral *Nq. pachyderma.*

Several intervals bear more than 10% dextral forms of the species. An interval of seven samples at Hole 856A contains the dextral form (88% to 11% sinistral forms) from 16.77 ± 0.84 to 20.06 ± 0.56 mbsf (Fig. 4). The samples (Fig. 5) also contain high frequencies of *Turborotalita quinqueloba* and species from the transitional watermass, including *Globorotalia hirsuta, Globorotalia inflata, Globigerinoides ruber, Globoturborotalita rubescens, Turborotalita humilis, Tenuitella iota*, and *Orbulina universa.* Only one of the seven samples is clearly turbiditic (Sample 856A-3H-5, 108–110 cm), and the others are probably hemipelagic (Table 1) based on sand content, lithology, and constituents of the sand-size fraction. Two intervals bear dextral forms at Hole 857A (Fig. 4): (1) one sample bearing 78% sinistral forms lies at 26.89 mbsf and (2) nine samples with 8% to 81% sinistral forms lie between 36.16 ± 0.17 and 40.37 ± 0.21 mbsf. The depositional style of the first interval is ambiguous (Table 2) and will be discussed in a later section. The second interval (Fig. 6) also contains high frequencies of *Turborotalita quinqueloba* and species from the transitional watermass including *Globorotalia hirsuta, Globorotalia inflata, Globigerinoides ruber, Globoturborotalita rubescens, Turborotalita humilis, Tenuitella iota*, and *Orbulina universa.* Five of the nine samples are turbiditic and four are probably hemipelagic (Table 2) based on sand content, lithology, and constituents of the sand-size fraction.

An unusual sample of abundant recrystallized planktonic foraminifers is preserved at 375 mbsf in Hole 857C. The assemblage consists of 47% sinistral *Nq. pachyderma*, 2% dextral *Nq. pachyderma*, 20% *Globigerina bulloides*, 2% *Globigerinita glutinata*, and 29% indeterminate specimens that could not be identified due to their poor preservation state.

Paleoenvironmental Analysis

The census of planktonic foraminifers in the 103 samples that contain abundant tests from Holes 856A and 857A tabulates species typical of well-preserved assemblages from cool temperate to subpolar water masses (Table 6). Twenty-one taxa are listed, including sinistral *Nq. pachyderma, Globigerina bulloides, Turborotalita quinqueloba, Globigerinita glutinata, Globigerinita uvula, Globigerinita* cf. *uvula, Globigerinita minuta*, dextral *Nq. pachyderma, Orbulina universa, Tenuitella iota, Tenuitella parkerae, Globorotalia scitula, Globorotalia* sp. A, a juvenile, nonencrusted sinistral *Nq. pachyderma, Globorotalia theyeri, Globigerina falconensis, Globorotalia inflata, Globorotalia hirsuta, Globigerinoides ruber, Globoturborotalita rubescens, Turborotalita humilis*, and indeterminate specimens (Table 6, and "Taxonomic Notes" section, this chapter). The first seven taxa are common (Figs. 5 and 6) and the latter taxa are infrequent. In all subsequent discussions, *Globigerinita uvula, Globigerinita* cf. *uvula*, and *Globigerinita minuta* are considered one counting group called *Globigerinita uvula* (see "Taxonomic Notes" section, this chapter).

Inspection of Figures 7 and 8 shows several distinctive trends. On average, samples from Hole 856A have 17% more sinistral *Nq. pachyderma* and fewer *Ga. bulloides, Tr. quinqueloba*, and *Gt. uvula* than those from Hole 857A. At Hole 856A, sinistral *Nq. pachyderma* increase in relative frequency below 22 mbsf while frequencies of *Ga. bulloides* and *Tr. quinqueloba* decrease. This effect occurs 4 m below the shallowest occurrence of carbonate concretions and 2 m below the shallowest common occurrence of calcite overgrowths on foraminif-

Table 5. Selection of Holocene-Pleistocene boundaries.

Core, section, interval (cm)	Depth (mbsf)	Tl	Pdl	Pdr	Coil	Age
139-855A-						
1R-1, 0–1	0.00	30	23	7	77	Holocene
1R-1, 100–102	1.00	30	25	5	83	Holocene
1R-2, 98–100	2.48	31	31	0	100	Pleistocene
1R-3, 102–104	4.02	30	30	0	100	Pleistocene
1R-4, 102–104	5.52	30	28	2	93	Pleistocene
1R-5, 71–73	6.71	30	30	0	100	Pleistocene
1R-CC	7.60	31	26	5	84	Turbidite
2R-1, 118–120	8.78	0	0	0		Barren
2R-2, 138–140	10.48	30	30	0	100	Pleistocene
2R-3, 118–120	11.78	0	0	0		Barren
2R-4, 60–62	12.70	0	0	0		Barren
2R-5, 56–60	14.16	30	30	0	100	Pleistocene
2R-CC	16.60	30	28	2	93	Pleistocene
139-855C-						
1R-1, 0–1	0.00	30	27	3	90	Holocene(?)
1R-1, 89–91	0.89	30	25	5	83	Holocene
1R-2, 55–57	2.05	30	29	1	97	Pleistocene
1R-3, 90–92	3.90	30	30	0	100	Pleistocene
1R-4, 92–94	5.42	30	30	0	100	Pleistocene
1R-5, 92–94	6.92	30	28	2	93	Pleistocene
1R-6, 79–81	8.29	0	0	0		Barren
1R-CC	8.70	31	30	1	97	Pleistocene
139-856A-						
1H-1, 0–1	0.00	75	64	11	85	Holocene
1H-1, 91–93	0.91	58	56	2	97	Pleistocene
1H-2, 48–50	1.68	140	136	4	97	Pleistocene
2H-2, 90–92	5.10	201	199	2	99	Pleistocene
139-856B-						
1H-1, 0–1	0.00	30	30	0	100	Pleistocene
1H-1, 89–91	0.89	30	28	2	93	Pleistocene
139-857A-						
1H-1, 0–1	1.90	114	97	17	85	Holocene
1H-1, 79–81	2.69	149	144	5	97	Pleistocene
1H-2, 125–129	4.65	152	150	2	99	Pleistocene
1H-3, 10–13	5.00	94	94	0	100	Pleistocene
139-857B						
1H-1, 0–1	0.00	30	18	12	60	Holocene
1H-1, 80–82	0.80	30	25	5	83	Holocene
1H-2, 17–19	1.67	30	29	1	97	Pleistocene
1H-3, 10–12	3.10	30	30	0	100	Pleistocene
139-857C-						
1R-1, 0–1	0.00	30	13	17	43	Holocene
1R-1, 61–65	0.61	30	22	8	73	Holocene
1R-2, 16–18	1.66	30	29	1	97	Pleistocene
1R-3, 31–33	3.31	0	0	0		Barren
1R-CC	3.40	30	28	2	93	Pleistocene
139-858A-						
1H-1, 0–1	0.00	30	18	12	60	Holocene
1H-1, 48–50	0.48	30	26	4	87	Pleistocene
1H-CC	2.40	31	31	0	100	Pleistocene
139-858B-						
1H-1, 0–1	0.00	0	0	0		Barren
1H-1, 89–93	0.89	30	30	0	100	Pleistocene
139-858C-						
1H-1, 0–1	0.00	37	28	9	76	Holocene
1H-1, 120–124	1.20	31	30	1	97	Pleistocene
139-858D-						
1H-1, 0–1	0.00	0	0	0		Barren
1H-1, 37–41	0.37	0	0	0		Barren
1H-2, 60–64	2.10	30	30	0	100	Pleistocene

Notes: Tl = total number of specimens counted; Pdl = number of sinistral *Neogloboquadrina pachyderma* counted; Pdr = number of dextral *Neogloboquadrina pachyderma* counted; Coil = coiling ratio (100 · Pdl/Tl).

eral tests. Hole 856A also has more indeterminate species than Hole 857A, an effect which is in part due to the calcite overgrowths on foraminiferal tests.

Q-mode cluster analysis (Tables 7, 8, and 9; Fig. 9) resolves three major groups of samples, Cluster 1 with 34 samples that contain more than 43% sinistral *Nq. pachyderma* and lower frequencies of other species; Cluster 2 with six samples that contain very low frequencies (<4%) of sinistral *Nq. pachyderma*, significant frequencies of dextral *Nq. pachyderma, Gt. glutinata*, and transitional species, and high frequencies of *Tr. quinqueloba*; and Cluster 3 with 63 samples that contain 41% to 7% sinistral *Nq. pachyderma.* Clusters 1 and 3 are further divided into subclusters. Cluster 1 has two subclusters, a and b, distinguished primarily by higher and lower frequencies of sinistral *Nq. pachyderma.* Cluster 3 is divided into three subclusters, a, b, and c. Subcluster 3a has the most equitable distribution of frequencies among sinistral *Nq. pachyderma, Tr. quinqueloba*, and *Gt. uvula.* Subcluster 3b has moderate frequencies of *Tr. quinqueloba* and sinistral *Nq. pachyderma* and relatively low frequencies of *Gt. uvula.* Subcluster 3c has high frequencies of *Gt. uvula*, moderate frequencies of sinistral *Nq. pachyderma*, and fairly low frequencies of *Tr. quinqueloba.*

Correlation analysis supports the relationships discussed above (Table 10). Frequencies of six of the seven taxonomic groups show some correlations with other groups. Sinistral *Nq. pachyderma* correlates negatively with *Tr. quinqueloba, Gt. uvula,* and *Gt. glutinata.* Dextral *Nq. pachyderma* correlates positively with *Gt. glutinata* and the transitional species and negatively with *Gt. uvula. Gt. glutinata* correlates positively with the transitional species. These relationships are seen in the cluster associations. Relative frequencies of *Ga. bulloides*, however, do not correlate significantly with those of any other species and play no clear role in clustering the samples.

At Hole 856A (Figs. 7 and 8), Cluster 1 dominates faunas below 22 mbsf within the zone of calcite precipitation, but does not dominate below the shallowest occurrence of diagenetic carbonate (46.05 mbsf) at Hole 857A. Cluster 2 dominates at one discrete interval in each of Holes 856A and 857A. Cluster 3 dominates throughout the remainder of the fossil-rich sequences.

DISCUSSION

Biostratigraphy

The intervals of sinistral and dextral coiling of *Nq. pachyderma* were used to subdivide the fossil-rich sequences in Hole 856A and 857A (Fig. 4). The surficial interval bearing dextral forms of the species is tentatively called coiling direction zone 1; the underlying interval of >90% sinistral forms, coiling direction zone 2; the underlying interval dominated by the dextral form, coiling direction zone 3; and the underlying interval of >90% sinistral forms, coiling direction zone 4. The intervals from 16.77 to 20.06 mbsf at Hole 856A and the interval from 36.16 to 40.37 mbsf at Hole 857A are tentatively correlated and assigned to coiling direction zone 3 based on the similarity of their assemblages. The samples cluster together in the cluster analysis (Table 7, Cluster 2) based on the most common species. Inspection of the species present from the transitional and subtropical water masses again shows great similarities (Table 6; Figs. 5 and 6).

Hole 857A has one other subsurface "interval" of dextral coiling forms (78% sinistral forms) represented by Sample 857A-4H-4, 49–51 cm, from 26.89 mbsf (Fig. 4). The samples from 10 cm below and 8 cm above have 100% and 90% sinistrally coiled forms, respectively. The sample is unusual compared with others in the data set (Fig. 6); it contains the highest frequency of *Ga. bulloides*, and it does not cluster stably when other amalgamation methods are used. It has the fifth highest benthic foraminiferal frequency, and it was taken from the top of a fining upward sequence. The unusual sample is excluded from biostratigraphic assignment.

Two datums were tentatively recognized at Holes 856A and 857A: the base of the Holocene and the base of the penultimate interglacial period (= base of Oxygen Isotope Stage 5). I assume that the base of coiling direction zone 1 marks the base of the Holocene at about 11,000 yr ago in the North Pacific Ocean (Bandy, 1960). Please note that the assumption may be incorrect and is presently under study (see "Biostratigraphy of the Northeast Pacific Ocean" section, this chapter). The depths of the Holocene-Pleistocene boundary (Table 4) range from a minimum of less than 0.49 mbsf at Site 858 to a maximum between 0.81 and 2.49 mbsf at the other sites, discounting Hole 857A, at which

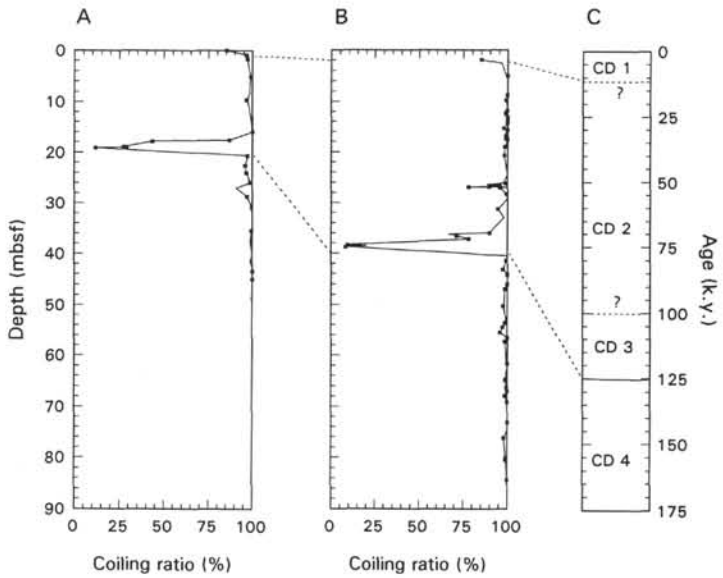

Figure 4. Coiling ratios of samples in (**A**) Hole 856A and (**B**) Hole 857A measured as the frequency of sinistral *Neogloboquadrina pachyderma* (Ehrenberg) relative to both sinistral and dextral forms. Hemipelagic(?) samples are flagged by filled squares; turbiditic samples have no symbol. The cores are correlated by dashed lines to informal coiling direction zones (**C**).

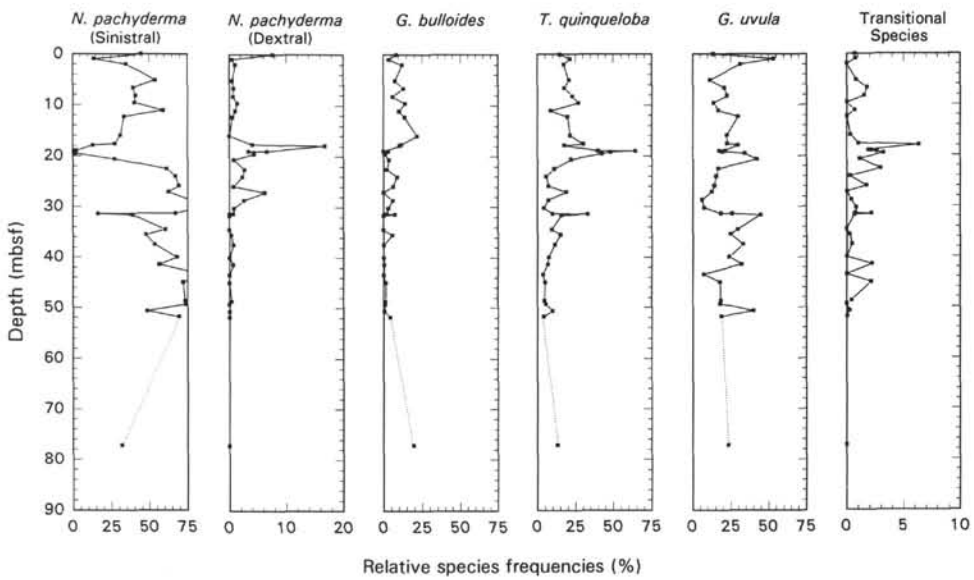

Figure 5. Relative frequencies (%) of six common taxa at Hole 856A plotted with depth in hole (mbsf).

there were operational difficulties that make the true depth uncertain and Hole 856B where the uppermost part of the section was eroded. The depths of the boundary at Sites 855, 856A, and 857 are not significantly different due to the coarse sampling interval (see Table 4, "Stratigraphic error" column). The average depth of the boundary is 0.94 ± 0.50 m and the average sedimentation rate for the Holocene at Leg 139 sites is 9 ± 4 cm/k.y., which is comparable to the rate of 11.5 cm/k.y. determined by Al-Aasm and Blaise (1991) for one core in Middle Valley, the average rate of 14 ± 4 cm/k.y. estimated in Escanaba Trough (Karlin and Lyle, 1986), and the rate of 10 cm/k.y. estimated in intercanyon areas of Astoria Fan (Nelson et al., 1968). Differences in sedimentation rates, however, should be regarded with caution because differences in sampling methods can cause differences in plastic compaction and extension during coring.

I assume that the base of the coiling direction zone 3 marks the base of the penultimate interglacial period (= Oxygen Isotope Stage 5) at 125,000 yr ago. The sedimentation rate from the Holocene-Pleistocene boundary to this datum is 17 cm/k.y. at Hole 856A and 33 cm/k.y. at Hole 857A (Table 11). These rates are similar to the average Pleistocene rate calculated on Astoria Fan at Deep Sea Drilling Project Site 174. The interval between the datum levels at Hole 856A lies almost entirely in Lithologic Subunit IIA, so the sedimentation rate may be relatively constant throughout the interval. The interval between the datum levels at Hole 857A lies both in Lithologic Unit I and Lithologic Subunit IIA, which contains more frequent and coarser turbidites than the overlying unit. The sedimentation rate is probably faster below the lithologic boundary at 25.20 mbsf. The lithologic boundary probably marks the age of an uplift event at the section. The age from simple interpolation suggests that this event occurred between 80,000 and 125,000 yr ago.

The ages of the bases of the fossil-rich intervals were estimated at Hole 856A and 857A. The accuracy of the extrapolation is highly suspect, but it does provide maximum expected ages of 302,000 yr at Hole 856A and 248,000 yr at Hole 857A. (For comparison, the estimated age of basement is 320,000 and 250,000 yr, respectively, at Holes 856A and 857A.) If the extrapolated ages were correct, then the fossil-rich sequences should each contain an additional interglacial fauna from the base of Oxygen Isotope Stage 7 from 240,000 yr ago.

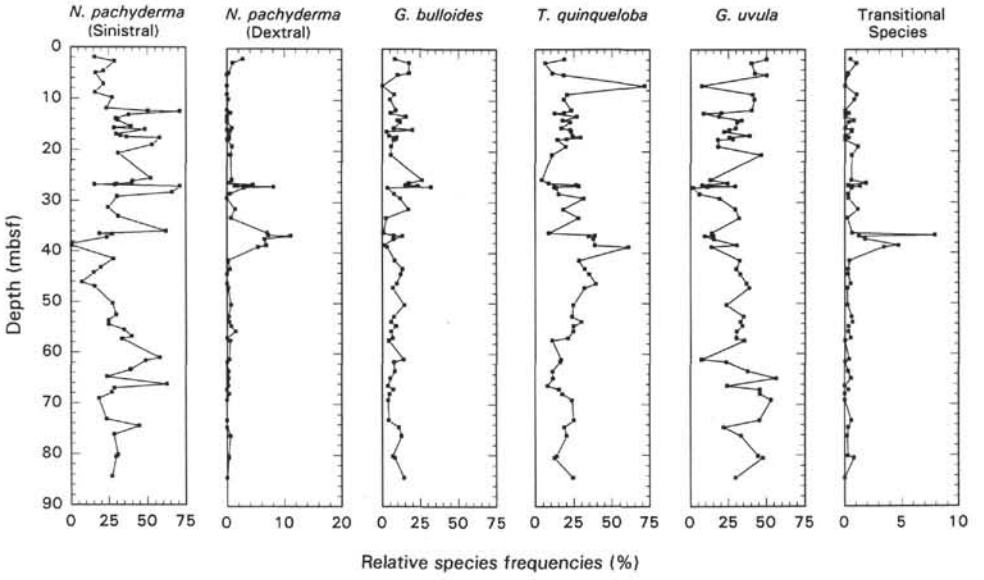

Figure 6. Relative frequencies (%) of six common taxa at Hole 857A plotted with depth in hole (mbsf).

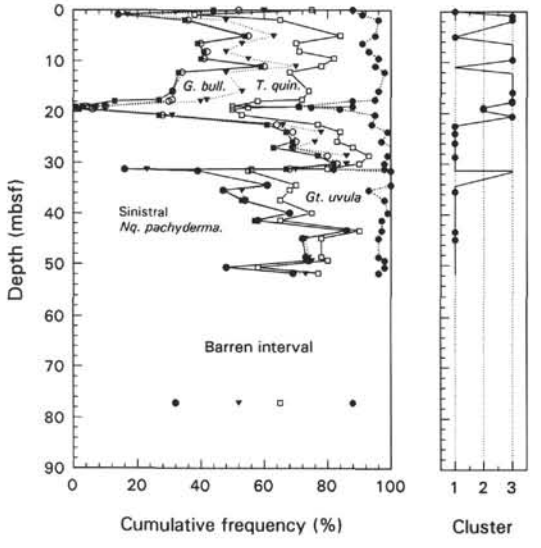

Figure 7. Cumulative frequencies (%) of four common taxa (left graph) and clusters from Q-mode analysis (right graph) plotted with depth (mbsf) at Hole 856A. The four common taxa are sinistral *Neogloboquadrina pachyderma*, *Globigerina bulloides*, *Turborotalita quinqueloba*, and *Globigerinita uvula*. Cluster 1 includes all samples from the subarctic dissolution assemblage, Cluster 2 includes all samples from the transitional assemblage, and Cluster 3 includes all samples from the subarctic assemblage. In the right graph, hemipelagic(?) samples are flagged by filled circles and turbiditic samples have no symbol.

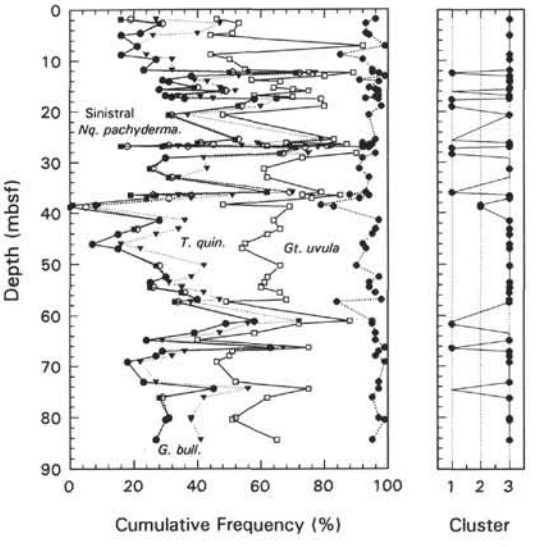

Figure 8. Cumulative frequencies (%) of four common taxa (left graph) and clusters from Q-mode analysis (right graph) plotted with depth (mbsf) at Hole 857A. The four common taxa are sinistral *Neogloboquadrina pachyderma*, *Globigerina bulloides*, *Turborotalita quinqueloba*, and *Globigerinita uvula*. Cluster 1 includes all samples from the subarctic dissolution assemblage, Cluster 2 includes all samples from the transitional assemblage, and Cluster 3 includes all samples from the subarctic assemblage. In the right graph, hemipelagic(?) samples are flagged by filled circles and turbiditic samples have no symbol.

No such interval was found, but additional samples are presently under study. It is possible that a dextral coiling interval was missed during sampling. The observed dextral intervals span 2.21 and 4.21 m in Holes 856A and 857A, respectively, and sampling intervals average 1.55 m in Hole 856A and 1.09 m in Hole 857A. Therefore, a dextral coiling shift shorter than these sampling intervals would be entirely missed.

The sedimentary sequences below 85 mbsf at most Leg 139 holes were mostly barren or depleted of fossils and could not be zoned. One fossil-rich sample, though highly recrystallized, was recovered from 375 mbsf in Hole 857C (857C-40R-CC). The sample bears an assemblage that is consistent with cold-water faunas of the last 0.6 Ma in the subarctic Pacific Ocean (Lagoe and Thompson, 1988).

Paleoenvironment

The assemblages defined by cluster analysis are typical of the transitional and subpolar plankton assemblages (Bradshaw, 1959) that have been modified by dissolution (Coulbourn et al., 1980; Sautter and Thunell, 1989; 1991). Cluster 1 (Fig. 9) is dominated by sinistral *Nq. pachyderma* and is typical of subpolar assemblages modified by dissolution so that delicate species have been removed (Sautter and Thunell,

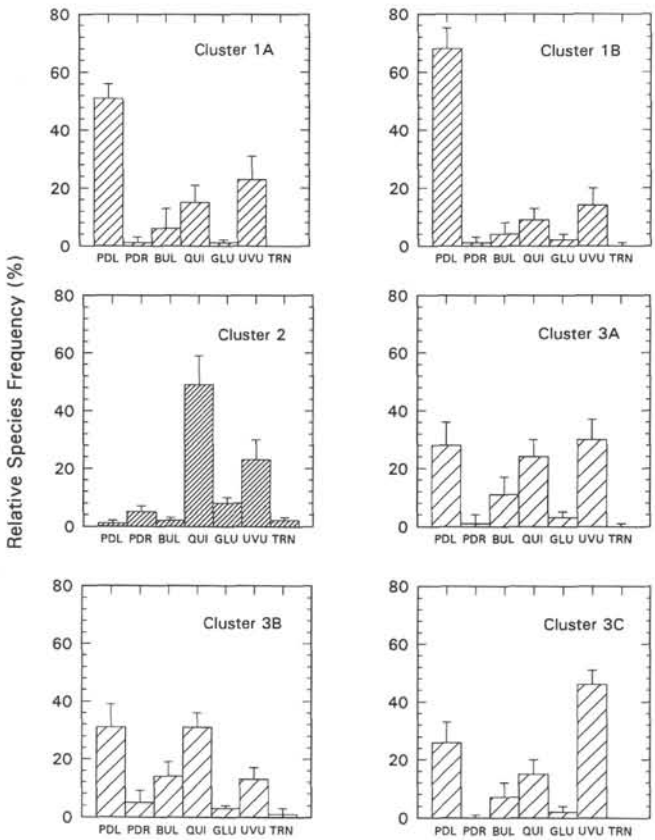

Figure 9. Average species composition of each subcluster from the Q-mode cluster analysis of samples (Table 8). The standard deviation for each species average is shown by the error bars. The subarctic dissolution assemblage (Cluster 1) is marked by an intermediate diagonal line, the transitional assemblage (Cluster 2) is marked by the fine diagonal line, and the subarctic assemblage (Cluster 3) is marked by a coarse diagonal line. Abbreviations are as in Table 8.

1989; 1991). This is consistent with the fact that most of the samples in the cluster come from the zone of calcite overgrowths in Hole 856A. Some of the delicate forms apparently were removed by postdepositional calcite mobilization. These assemblages are similar to those at Hole 857A which lie both above and below the depth of the first diagenetic carbonate at 46.05 mbsf. The assemblages altered by overgrowths are indistinguishable in species content from those dissolved by ordinary postdepositional processes.

Cluster 2 (Fig. 9) is typical of a transitional assemblage with more dextral than sinistral *Nq. pachyderma* and the common occurrence of other subpolar species. Compared to the rest of the data set, the samples have the most abundant frequencies of dextral *Nq. pachyderma*, *Tr. quinqueloba*, and *Gt. glutinata*, species which undergo maximum production together at times of maximum oceanic fertility (Sautter and Thunell, 1991). Maximum production of *Tr. quinqueloba*, in particular, is associated with spring bloom conditions (Sautter and Sancetta, 1992). Proximity to the subarctic boundary is suggested by small but significant occurrences of cool subtropical taxa such as *Globorotalia hirsuta*, *Globorotalia inflata*, *Globigerinoides ruber*, and *Globoturborotalita rubescens*. The assemblage also appears fairly well preserved based on the large numbers of delicate species relative to robust *Nq. pachyderma* and based on planktonic foraminiferal numbers that are not significantly different from those of the glacial faunas.

Cluster 3 (Fig. 9) is typical of subarctic assemblages that are better preserved than those of Cluster 1 (Sautter and Thunell, 1989). The assemblage has significantly more delicate species and fewer of the robust sinistral *Nq. pachyderma* than Cluster 1. It is unclear whether the dominance of *Tr. quinqueloba* (Cluster 3b), *Gt. uvula* (Cluster 3c), or the more equitable preservation of both these species with *Ga. bulloides* (Cluster 3a) is controlled by environment of the water mass (changes in upwelling [Lyle et al., 1992], freshening [Sancetta, 1979], or cooling [Moore et al., 1980] of surface waters as discussed in the "Pleistocene Paleoenvironmental History" section, this chapter), or by postdepositional dissolution.

The species *Globigerina bulloides* occurs in both high and low frequencies in most of the subclusters. The species has wide environmental tolerances, thrives in water masses from subtropical to subpolar regions, and reaches peaks of production during upwelling events (Sautter and Thunell, 1991; Sautter and Sancetta, 1992). The tests are also very susceptible to dissolution (Sautter and Thunell, 1989; 1991), and their frequency may be sensitive to postdepositional processes. For all of these reasons, it is not surprising that the species does not correlate with any other subarctic species and does not aid clustering of samples.

The patterns of clusters with depth in hole (Figs. 7 and 8) map out several environmental events:

1. The appearance of the transitional assemblage (Cluster 2) at the Leg 139 sites suggests that transitional waters in proximity to the subpolar boundary migrated to this locality at least once during the late Pleistocene. I tentatively correlate the migration to the penultimate interglacial period 125,000 yr ago.
2. In general, well-preserved assemblages of subarctic foraminifers (Cluster 3) occur above 22 mbsf at Hole 856A and throughout Hole 857A with sporadic occurrences of the dissolution subarctic assemblage (Cluster 1). The distributions of these assemblages reflect the position of the regional CCD. The regional CCD lay below Leg 139 sites throughout most of the two late Pleistocene glacial periods observed at the study site. It is unclear whether the sporadic occurrences of the dissolution assemblage in well-preserved intervals is related to brief rises of the CCD (Karlin et al., 1992). The dissolution assemblage dominates samples below 22 mbsf at Hole 856A and reflects a zone of calcite precipitation driven by hydrothermal alteration.
3. The specimens in coiling direction zone CD 3 (penultimate interglacial period) appear fairly well preserved, indicating that the CCD did not rise above the sites at about 2400 m water depth as the CCD did not rise above the sites during the present interglacial period.

CONCLUSIONS

1. The late Quaternary sequences were divided into four informal coiling direction zones numbered from the top to the bottom of the fossil-rich sections. Coiling direction zones 1 and 3 contain fewer than 90% sinistrally coiled forms of *Nq. pachyderma* and coiling direction zones 2 and 4 contain more than 90% sinistrally coiled forms.
2. Coiling direction zones 1 and 3 correspond approximately to interglacial intervals: a Holocene interval at the tops of Holes 856A and 857A and a penultimate interglacial interval with bases at approximately 20 and 40 mbsf in Holes 856A and 857A, respectively. The bases of these intervals are tentatively assigned ages of 11,000 and 125,000 yr ago.
3. The census data of Pleistocene planktonic foraminifers cluster into three main groupings: (1) a subarctic dissolution assemblage from which delicate forms have been dissolved, (2) a transitional assemblage with species characteristic of transitional waters which presently lie south of Leg 139 sites, and (3) a subarctic assemblage with 3 subclusters which reflect differences either in surface-water environment or postdepositional dissolution.
4. Foraminifers below 22 mbsf at Hole 856A are covered by calcite overgrowths and the assemblage has been modified by removal of delicate species. Most samples in this interval belong to the subarctic dissolution assemblage, Cluster 1.
5. The interglacial interval is characterized by the transitional assemblage which suggests that the subpolar boundary migrated north-

Table 6. Census (tests counted in a split of the sample) of planktonic foraminifers at Holes 856A and 857A.

Core, section, interval (cm)	Depth (mbsf)	Split	SedWt	SandWt	Ben	Pla	Pdl	Pdr	Bul	Qui	Glu	Cfu	Uvu	Uni	Iot	Par	Juv	Ind	Sci	Gra	Min	The	Fal	Inf	Hum	Rub	Hir	Rube
139-856A-																												
1H-1, 0–1	0.00	0.0939			188	144	64	11	12	21	7	11	3	1	0	0	0	9	0	0	5	0	0	0	0	0	0	0
1H-1, 91–93	0.91	0.0059	8.3919	0.1289	9	404	56	2	14	86	13	129	26	0	1	0	3	12	2	0	60	0	0	0	0	0	0	0
1H-2, 48–50	1.68	0.0078	10.0561	0.1854	8	392	136	4	47	67	11	97	15	0	0	0	4	1	0	0	10	0	0	0	0	0	0	0
2H-2, 90–92	5.10	0.1875	11.7541	0.0354	149	369	199	2	28	76	12	30	6	0	1	0	1	6	2	0	6	0	0	0	0	0	0	0
2H-3, 90–92	6.60	1.0000	13.5487	0.0085	23	292	114	2	37	51	17	39	2	2	3	0	0	6	0	0	19	0	0	0	0	0	0	0
2H-4, 101–103	8.21	0.0781	12.7467	0.0506	72	337	137	2	19	77	8	51	9	0	0	0	0	14	3	0	15	0	0	0	2	0	0	0
2H-5, 86–88	9.56	0.1875	11.9664	0.0310	275	295	118	4	41	79	10	25	6	0	0	0	1	2	0	0	9	0	0	0	0	0	0	0
2H-6, 86–88	11.06	0.0234	11.6165	0.0703	15	308	182	3	31	26	8	37	7	0	0	0	1	3	1	0	8	0	0	0	1	0	0	0
2H-7, 56–58	12.26	0.0313	9.7456	0.0828	8	588	195	3	80	115	14	168	0	0	0	0	0	7	0	0	6	0	0	0	0	0	0	0
3H-2, 90–95	14.60	1.0000	13.4915	0.0079	0	0	0	0	0	0	0	0	0	0	0	0	0	0	0	0	0	0	0	0	0	0	0	0
3H-3, 72–74	15.92	0.1250	14.1628	0.0234	34	327	101	0	71	70	7	67	2	0	0	0	0	4	1	0	4	0	0	0	0	0	0	0
3H-4, 91–93	17.61	0.0938	13.9345	0.0382	28	297	81	12	34	90	7	33	0	0	0	0	0	3	3	0	34	0	0	0	0	0	0	0
3H-4, 117–119	17.87	0.0469	12.6937	0.0882	34	363	47	61	38	64	18	54	4	0	1	0	1	3	3	1	50	0	0	17	0	1	0	0
3H-5, 74–76	18.94	0.1250	10.9087	0.0209	117	317	8	21	0	127	30	47	15	0	0	22	17	18	0	0	6	0	0	1	0	5	0	0
3H-5, 78–80	18.98	0.1250	9.8233	0.0326	75	508	7	17	16	327	29	69	3	0	1	0	0	13	10	0	16	0	0	0	0	0	0	0
3H-5, 96–98	19.16	0.0781	11.6319	0.0562	47	346	2	15	6	167	25	37	10	0	2	17	17	20	2	2	21	0	2	1	0	0	0	0
3H-5, 130–132	19.20	0.0625	12.0175	0.0745	42	621	11	27	6	264	38	199	8	0	2	11	18	13	1	0	6	0	0	0	13	2	1	1
3H-6, 92–94	20.62	0.0039	11.7012	0.5064	38	539	146	4	18	118	8	134	2	0	2	0	0	12	3	1	91	0	0	0	0	0	0	0
3H-7, 39–41	21.59	1.0000	14.4733	0.0887	0	0	0	0	0	0	0	0	0	0	0	0	0	0	0	0	0	0	0	0	0	0	0	0
4H-1, 82–84	22.52	0.0625	12.6838	0.0953	132	308	189	8	6	33	6	39	0	0	0	0	0	5	1	0	12	0	8	0	0	0	0	0
4H-2, 81–83	24.01	0.0625	16.8037	0.1962	54	798	535	18	70	44	4	64	2	0	0	0	0	3	0	0	56	0	2	0	0	0	0	0
4H-3, 122–124	25.92	0.0313	14.7037	0.2035	16	709	492	5	43	51	2	55	11	0	0	0	0	4	0	1	34	0	11	0	0	0	0	0
4H-4, 88–90	27.08	0.0313	17.8245	0.1579	4	16	10	1	0	3	0	2	0	0	0	0	0	0	0	0	0	0	0	0	0	0	0	0
4H-5, 96–98	28.66	0.0156	12.8155	0.4296	23	789	606	20	46	56	6	21	1	0	0	0	0	5	2	0	25	0	0	1	0	0	0	0
4H-6, 108–110	30.23	0.0156	15.5024	2.0099	35	369	302	3	11	15	6	9	2	0	0	0	0	1	2	1	17	0	0	0	0	0	0	0
4H-7, 62–64	31.32	0.1250	16.5603	0.0750	33	923	621	6	19	91	5	73	13	0	0	0	0	4	5	0	84	0	2	0	0	0	0	0
5H-1, 19–21	31.39	0.0078	14.8123	0.5084	10	462	75	0	34	153	11	100	5	0	0	0	0	60	10	0	14	0	0	0	0	0	0	0
5H-2, 6–8	31.64	0.0625	18.5638	0.2457	506	307	119	0	0	48	0	44	8	0	0	0	0	1	2	0	85	0	0	0	0	0	0	0
5H-3, 135–137	34.43	0.0469	14.0245	1.3818	172	223	135	0	0	21	0	37	2	0	0	0	0	1	0	0	27	0	0	0	0	0	0	0
5H-4, 88–90	35.46	0.0078	14.0805	0.4416	8	434	206	1	24	65	4	86	6	0	0	0	0	26	1	0	15	0	0	0	0	0	0	0
5H-5, 133–135	37.41	0.0626	16.8116	0.3300	285	454	242	3	0	51	0	70	14	0	0	0	0	6	0	0	66	0	2	0	0	0	0	0
5H-6, 90–92	38.48	1.0000	18.0135	0.1189	0	0	0	0	0	0	0	0	0	0	0	0	0	0	0	0	0	0	0	0	0	0	0	0
5H-7, 88–90	39.96	0.0352	18.0146	0.6291	415	301	205	0	0	22	0	26	5	0	0	0	0	2	0	0	41	0	0	0	0	0	0	0
6H-1, 68–70	41.38	0.0390	18.3194	0.4501	370	320	181	2	1	21	2	50	7	0	0	0	0	4	5	0	45	0	2	0	0	0	0	0
6H-2, 123–125	43.43	0.1250	13.4379	0.0308	83	28	24	0	0	1	0	0	0	0	0	0	0	1	0	0	2	0	0	0	0	0	0	0
6H-3, 127–129	44.97	0.0078	14.0708	0.3310	27	425	306	0	6	21	4	48	4	0	0	0	0	3	2	5	24	0	1	0	1	0	0	0
6H-6, 46–48	48.66	0.0625	16.1224	0.0301	277	245	180	1	3	11	1	18	2	0	0	0	0	3	0	0	25	0	1	0	0	0	0	0
6H-6, 112–114	49.32	0.1250	15.0945	0.2084	20	204	151	0	2	11	0	19	1	0	0	0	0	3	0	0	17	0	0	0	0	0	0	0
7H-1, 48–50	50.68	0.1563	10.6923	0.4998	281	457	221	0	1	44	0	84	4	0	0	0	0	7	0	0	94	0	1	0	0	0	0	0
7H-2, 12–14	51.82	0.0313	11.0872	0.4418	52	364	252	0	15	14	4	57	8	0	0	0	0	11	0	0	3	0	0	0	0	0	0	0
7H-2, 101–103	52.71	1.0000	15.6216	3.1759	0	0	0	0	0	0	0	0	0	0	0	0	0	0	0	0	0	0	0	0	0	0	0	0
7H-4, 64–66	55.34	1.0000	9.5226	2.5750	0	0	0	0	0	0	0	0	0	0	0	0	0	0	0	0	0	0	0	0	0	0	0	0
7H-4, 94–96	55.64	1.0000	17.2013	0.9476	0	0	0	0	0	0	0	0	0	0	0	0	0	0	0	0	0	0	0	0	0	0	0	0
7H-5, 46–48	56.66	1.0000	18.2152	3.0830	0	0	0	0	0	0	0	0	0	0	0	0	0	0	0	0	0	0	0	0	0	0	0	0
7H-6, 39–41	58.09	1.0000	12.2123	0.5833	0	0	0	0	0	0	0	0	0	0	0	0	0	0	0	0	0	0	0	0	0	0	0	0
7H-7, 23–25	59.43	1.0000	18.7416	0.6284	0	0	0	0	0	0	0	0	0	0	0	0	0	0	0	0	0	0	0	0	0	0	0	0
8H-1, 87–90	60.57	1.0000	19.4122	0.0083	0	0	0	0	0	0	0	0	0	0	0	0	0	0	0	0	0	0	0	0	0	0	0	0
8H-2, 119–121	62.39	1.0000	15.9677	1.4649	0	0	0	0	0	0	0	0	0	0	0	0	0	0	0	0	0	0	0	0	0	0	0	0
8H-3, 120–123	63.90	1.0000	20.8706	0.0282	0	0	0	0	0	0	0	0	0	0	0	0	0	0	0	0	0	0	0	0	0	0	0	0
8H-4, 112–115	65.32	1.0000	20.3558	0.0717	0	0	0	0	0	0	0	0	0	0	0	0	0	0	0	0	0	0	0	0	0	0	0	0
8H-5, 98–101	66.68	1.0000	31.0085	0.8319	0	0	0	0	0	0	0	0	0	0	0	0	0	0	0	0	0	0	0	0	0	0	0	0
8H-6, 94–98	68.14	1.0000	24.6532	0.4317	0	0	0	0	0	0	0	0	0	0	0	0	0	0	0	0	0	0	0	0	0	0	0	0
9H-3, 90–92	73.10	1.0000	17.1721	0.0737	0	0	0	0	0	0	0	0	0	0	0	0	0	0	0	0	0	0	0	0	0	0	0	0
9H-4, 97–99	74.67	1.0000	17.6417	0.2727	0	0	0	0	0	0	0	0	0	0	0	0	0	0	0	0	0	0	0	0	0	0	0	0
9H-6, 46–48	77.16	1.0000	16.9033	0.0137	0	107	34	0	21	14	11	18	3	0	0	0	0	2	0	0	4	0	0	0	0	0	0	0
12X-1, 33–35	96.03	1.0000	15.0368	0.2781	0	0	0	0	0	0	0	0	0	0	0	0	0	0	0	0	0	0	0	0	0	0	0	0
12X-2, 32–34	97.52	1.0000	16.7443	1.6525	0	0	0	0	0	0	0	0	0	0	0	0	0	0	0	0	0	0	0	0	0	0	0	0

Table 6 (continued).

Core, section, interval (cm)	Depth (mbsf)	Split	SedWt	SandWt	Ben	Pla	Pdl	Pdr	Bul	Qui	Glu	Cfu	Uvu	Uni	Iot	Par	Juv	Ind	Sci	Gra	Min	The	Fal	Inf	Hum	Rub	Hir	Rube
139-857A-																												
1H-1, 0–1	1.90	0.0078			52	620	97	17	51	117	21	198	113	0	0	1	1	1	3	0	0	0	0	0	0	0	0	0
1H-1, 79–81	2.69	0.0313	12.5607	0.2305	11	506	144	5	89	32	5	128	75	0	0	5	8	10	1	4	0	0	0	0	0	0	0	0
1H-2, 125–129	4.65	0.0313	13.8467	0.1399	14	696	150	2	122	77	43	248	45	0	0	3	0	2	2	0	2	0	0	0	0	0	0	0
1H-3, 10–13	5.00	0.0078	12.6154	0.2284	6	577	94	0	58	106	11	191	98	0	0	14	0	4	1	0	0	0	0	0	0	0	0	0
1H-4, 72–76	7.12	1.0000	11.3201	0.0447	2	14	3	0	0	10	0	1	0	0	0	0	0	0	0	0	0	0	0	0	0	0	0	0
1H-5, 89–91	8.79	0.0078	9.5719	0.1230	3	398	63	0	31	81	31	112	51	0	0	23	0	2	4	0	0	0	0	0	0	0	0	0
1H-6, 36–38	9.76	0.0156	11.1513	0.1160	22	488	132	1	24	90	18	144	61	0	0	11	2	1	4	0	0	0	0	0	0	0	0	0
2H-1, 45–48	11.85	0.0039			29	385	90	0	34	89	11	130	25	0	0	1	3	2	0	0	0	0	0	0	0	0	0	0
2H-1, 97–99	12.37	0.0078	17.3152	0.2049	15	376	189	2	20	70	1	55	20	0	0	14	3	1	0	0	1	0	0	0	0	0	0	0
2H-1, 105–107	12.45	0.0313			34	330	234	2	18	41	3	18	10	0	0	0	1	2	0	1	0	0	0	0	0	0	0	0
2H-2, 20–22	13.10	0.0039			6	311	118	0	48	83	2	45	13	0	0	0	0	2	0	0	0	0	0	0	0	0	0	0
2H-2, 96–98	13.86	0.0078	16.8847	0.2345	17	395	116	0	39	70	15	14	118	0	0	17	1	1	2	0	1	1	0	0	0	0	0	0
2H-2, 129–131	14.19	0.0156			33	319	98	0	37	72	9	83	15	0	0	0	2	2	0	0	0	0	0	0	1	0	0	0
2H-3, 98–100	15.38	0.0625	20.5320	0.0296	22	457	179	4	34	76	22	36	100	0	0	2	0	4	0	0	0	0	0	0	0	0	0	0
2H-3, 129–131	15.69	0.0098			87	329	93	0	65	74	8	65	19	0	0	0	2	1	2	0	0	0	0	0	0	0	0	0
2H-4, 12–14	16.02	0.0625			64	347	167	2	9	80	8	65	11	0	0	0	2	1	1	0	0	0	0	0	1	0	0	0
2H-4, 98–100	16.88	0.0313	19.8153	0.0610	51	326	97	1	14	78	6	45	82	0	0	2	0	1	0	0	0	0	0	0	0	0	0	0
2H-4, 127–129	17.17	0.0234			86	305	99	1	28	89	7	68	10	0	0	0	1	1	1	0	0	0	0	0	0	0	0	0
2H-5, 7–9	17.47	0.0469	14.7550	0.0846	35	307	112	1	27	62	17	44	41	0	0	1	1	1	0	0	0	0	0	0	0	0	0	0
2H-5, 22–24	17.62	0.0078			24	323	187	0	24	46	7	48	10	0	0	0	0	1	0	0	0	0	0	0	0	0	0	0
2H-6, 9–11	18.99	0.0156			42	353	187	3	20	69	2	47	8	0	0	0	0	4	3	0	9	0	0	0	1	0	0	0
2H-7, 26–28	20.66	0.0313	15.4581	0.0656	42	346	107	2	19	37	9	123	37	0	0	4	3	3	1	1	0	0	0	0	0	0	0	0
4H-1, 124–126	23.14	1.0000	22.9955	0.3397	0	0	0	0	0	0	0	0	0	0	0	0	0	0	0	0	0	0	0	0	0	0	0	0
4H-2, 118–122	24.58	1.0000	22.3483	0.4102	0	0	0	0	0	0	0	0	0	0	0	0	0	0	0	0	0	0	0	0	0	0	0	0
4H-3, 64–66	25.54	0.7500	17.3573	0.0327	217	349	182	3	92	15	4	5	41	0	0	1	3	0	2	0	0	0	0	0	0	0	0	0
4H-3, 100–103	25.90	1.0000	24.8423	0.8424	0	0	0	0	0	0	0	0	0	0	0	0	0	0	0	0	0	0	0	0	0	0	0	0
4H-3, 125–127	26.15	0.0938	14.2653	0.0799	86	376	152	2	66	33	6	80	5	0	0	5	4	9	0	0	7	0	0	3	0	4	0	0
4H-4, 12–14	26.52	0.3750	12.5367	0.0926	404	328	131	15	50	87	14	22	2	0	0	3	0	2	0	0	1	0	0	0	0	1	0	0
4H-4, 30–32	26.70	1.0000	12.6680	0.1554	255	291	88	4	68	81	10	28	2	0	0	1	0	3	0	0	5	0	0	0	0	1	0	0
4H-4, 38–40	26.78	0.0625	12.7722	0.0827	42	448	70	8	73	126	25	108	11	0	0	0	3	4	1	0	14	0	4	0	0	1	0	0
4H-4, 49–51	26.89	0.0781			124	358	104	29	115	44	19	26	14	0	0	4	0	1	1	1	0	0	0	0	0	0	0	0
4H-4, 70–74	27.10	1.0000	16.7080	0.0187	471	170	121	5	6	23	11	2	1	1	0	0	0	0	0	0	0	0	0	0	0	0	0	0
4H-5, 40–44	28.30	0.0781	17.2686	0.0385	43	345	228	2	27	53	10	5	15	0	0	1	1	2	1	0	0	0	0	0	0	0	0	0
4H-5, 127–129	29.17	0.0313			60	306	93	0	36	96	10	54	2	0	0	3	0	8	1	0	3	0	0	0	0	0	0	0
4H-7, 43–47	31.33	0.0313	17.7345	0.0696	43	354	87	5	61	64	13	65	40	0	0	10	0	3	2	0	0	0	2	0	0	0	0	0
5H-2, 13–17	33.03	0.5000	22.6066	0.0195	99	456	142	3	11	127	12	114	33	0	0	2	3	8	0	1	0	0	0	0	0	0	0	0
5H-2, 38–42	33.28	1.0000	29.2689	0.6903	0	0	0	0	0	0	0	0	0	0	0	0	0	0	0	0	0	0	0	0	0	0	0	0
5H-3, 48–52	34.88	1.0000	25.5451	0.1559	0	0	0	0	0	0	0	0	0	0	0	0	0	0	0	0	0	0	0	0	0	0	0	0
5H-4, 9–13	35.99	0.2500			103	158	98	11	1	14	10	14	8	0	0	0	0	1	1	0	0	0	0	0	0	0	0	0
5H-4, 57–61	36.47	0.0625	19.5133	0.5970	105	317	60	23	24	123	9	39	8	0	0	1	1	3	3	0	0	0	0	22	0	0	0	0
5H-4, 70–72	36.60	0.4375	13.2702	0.0555	63	325	89	36	43	112	9	20	2	0	0	0	0	2	3	0	8	0	0	1	0	0	0	0
5H-4, 130–132	37.20	0.1250	12.6538	0.1188	112	336	79	22	25	127	14	43	7	0	1	5	0	6	4	0	2	0	0	0	1	0	0	0
5H-5, 105–107	38.45	0.1250	8.2780	0.0374	63	278	2	19	2	108	34	78	4	0	4	5	6	4	2	1	3	0	0	0	1	2	3	0
5H-5, 126–130	38.66	1.0000	16.2646	0.3497	0	0	0	0	0	0	0	0	0	0	0	0	0	0	0	0	0	0	0	0	0	0	0	0
5H-5, 140–142	38.80	0.0313	14.7918	0.1055	35	412	2	22	13	250	33	51	5	1	6	3	6	12	0	1	1	0	0	1	1	3	1	0
5H-6, 126–130	40.16	1.0000	25.7329	0.6689	0	0	0	0	0	0	0	0	0	0	0	0	0	0	0	0	0	0	0	0	0	0	0	0
5H-7, 18–22	40.58	1.0000	22.3659	0.3944	0	0	0	0	0	0	0	0	0	0	0	0	0	0	0	0	0	0	0	0	0	0	0	0
6H-1, 59–63	41.49	0.0078	21.1804	0.2023	5	519	145	1	42	146	12	119	49	0	0	0	2	0	2	0	1	0	0	0	0	0	0	0
6H-2, 76–80	43.16	0.0195	23.0630	0.2720	4	363	71	2	48	116	7	75	33	0	0	6	0	3	1	0	1	0	0	0	0	0	0	0
6H-3, 27–31	44.17	0.0059			10	407	62	0	49	142	7	102	31	0	0	10	1	2	0	1	0	0	0	0	0	0	0	0
6H-4, 66–70	46.06	0.0078			11	392	28	0	37	154	14	115	30	0	2	4	0	8	0	0	0	0	0	0	0	0	0	0
6H-5, 4–8	46.94	0.1250			30	472	73	1	32	150	7	157	26	0	0	16	1	8	1	0	0	0	0	0	0	0	0	0
6H-5, 45–49	47.35	1.0000			0	0	0	0	0	0	0	0	0	0	0	0	0	0	0	0	0	0	0	0	0	0	0	0
6H-7, 38–42	50.28	0.0313			17	454	124	3	65	111	13	87	20	0	0	18	10	2	1	0	0	0	0	0	0	0	0	0
7H-3, 37–39	52.59	0.0156	24.6610	0.1054	22	345	102	1	26	82	5	108	13	0	0	1	2	3	2	0	0	0	0	0	0	0	0	0
7H-4, 1–5	53.63	0.0078			12	304	75	1	17	91	7	82	18	0	0	7	2	2	1	1	0	0	0	0	0	0	0	0
7H-4, 85–89	54.47	0.0020	26.7248	0.5848	3	304	75	2	27	75	4	99	5	0	0	10	4	2	1	0	0	0	0	0	0	0	0	0
7H-5, 75–79	55.52	0.0098	27.5015	0.1198	11	336	117	5	19	82	3	93	9	0	0	0	5	2	1	0	0	0	0	0	0	0	0	0
7H-6, 121–125	56.89	0.0156	26.2915	0.0795	17	402	160	0	27	85	2	107	13	0	0	4	0	1	2	0	1	0	0	0	0	0	0	0
7H-7, 28–32	57.35	1.0000	27.4537	0.0088	13	192	64	1	8	21	2	63	5	0	0	26	0	2	0	0	0	0	0	0	0	0	0	0
8H-1, 119–123	61.09	0.0098	18.9148	0.7795	6	297	172	1	41	49	2	17	4	0	0	6	2	2	1	0	0	0	0	0	0	0	0	0
8H-2, 21–25	61.61	0.0156	23.4379	0.1262	14	388	189	0	29	62	1	72	17	0	0	16	0	0	0	0	2	0	0	0	0	0	0	0

Table 6 (continued).

Core, section, interval (cm)	Depth (mbsf)	Split	SedWt	SandWt	Ben	Pla	Pdl	Pdr	Bul	Qui	Glu	Cfu	Uvu	Uni	Iot	Par	Juv	Ind	Sci	Gra	Min	The	Fal	Inf	Hum	Rub	Hir	Rube
8H-3, 54–58	63.44	0.0098	23.4246	0.3265	10	337	132	1	28	38	1	114	14	0	0	2	2	4	1	0	0	0	0	0	0	0	0	0
8H-4, 43–47	64.83	0.0156	22.8620	0.1423	34	723	172	2	38	83	5	373	35	0	1	7	4	0	3	0	0	0	0	0	0	0	0	0
8H-5, 40–44	66.30	0.0625	22.9083	0.0677	34	397	249	1	15	32	3	85	11	0	0	0	1	0	0	0	0	0	0	0	0	0	0	0
8H-5, 114–118	67.04	0.0078			5	305	87	0	22	47	2	112	27	0	0	2	2	3	0	0	0	0	0	0	1	0	0	0
8H-6, 52–56	67.92	0.0313	23.3108	0.0577	14	559	150	2	26	98	9	240	16	0	0	11	6	1	0	0	0	0	0	0	0	0	0	0
8H-7, 22–26	69.12	1.0000	24.3616	0.0495	75	185	34	0	7	44	1	82	16	0	0	1	0	0	0	0	0	0	0	0	0	0	0	0
9H-3, 74–80	73.14	0.0313	23.8800	0.0371	13	536	125	0	22	133	7	215	28	0	1	1	1	1	2	0	0	0	0	0	0	0	0	0
9H-4, 60–63	74.50	0.0469	20.2977	0.2926	18	331	148	0	36	62	5	65	7	0	0	1	1	5	1	0	0	0	0	0	0	0	0	0
9H-5, 79–84	76.19	0.0078			7	518	146	3	65	105	3	144	29	0	0	11	6	5	0	0	0	0	0	0	0	1	0	0
10H-1, 124–127	80.14	0.0625	17.4653	0.0224	11	382	117	1	26	53	6	152	18	0	0	5	3	0	1	0	0	0	0	0	0	0	0	0
10H-2, 12–14	80.52	0.0156			18	376	111	1	31	47	1	145	34	0	0	0	2	1	3	0	0	0	0	0	0	0	0	0
10H-4, 99–101	84.39	0.1875	19.6477	0.0149	8	346	93	0	49	84	7	90	13	0	0	2	4	4	0	0	0	0	0	0	0	0	0	0

Notes: Split = fraction of sample counted; SedWt = dry weight of bulk sediment; SandWt = dry weight of sand-size fraction; Ben = number of benthic foraminiferal tests; Pla = number of planktonic foraminiferal tests; Pdl = sinistral *Neogloboquadrina pachyderma*; Pdr = dextral *Neogloboquadrina pachyderma*; Bul = *Globigerina bulloides*; Qui = *Turborotalita quinqueloba*; Glu = *Globigerinita glutinata*; Cfu = *Globigerinita* cf. *uvula*; Uvu = *Globigerinita uvula*; Uni = *Orbulina universa*; Iot = *Tenuitella iota*; Par = *Tenuitella parkerae*; Juv = juvenile,, nonencrusted sinistral *N. pachyderma*; Ind = indeterminate specimens; Sci = *Globorotalia scitula*; Gra = *Globorotalia* sp. A; Min = *Globigerinita minuta*; The = *Globorotalia theyeri*; Fal = *Globigerina falconensis*; Inf = *Globorotalia inflata*; Hum = *Turborotalita humilis*; Rub = *Globoturborotalita rubescens*; Hir = *Globorotalia hirsuta*; Rube = *Globigerinoides ruber*.

ward to a position just south of the Leg 139 sites at 48°30′N latitude during the penultimate interglacial period. The sites constrain maximum northward migration of the subarctic boundary, but do not delimit the northern extent of transitional waters.

TAXONOMIC NOTES

Globigerina bulloides d'Orbigny
Globigerina bulloides d'Orbigny, 1826, ser. 1, v. 7, p. 277, nos. 17 and 76.

Globigerina clarkei Rögl and Bolli
Globigerina clarkei Rögl and Bolli, 1973, p. 563, pl. 4, figs. 13–15.
Note: This species was included in the *Tr. quinqueloba* counting group because it is difficult to distinguish from poorly preserved forms of the latter.

Globigerina falconensis Blow
Globigerina falconensis Blow, 1959, p. 177, pl. 9, figs. 40a–c, 41.

Globigerinita glutinata (Egger)
Globigerina glutinata Egger, 1893, p. 371, pl. 13, figs. 19–21.

Globigerinita minuta (Natland)
Globigerinoides minuta Natland, 1938, p. 150, pl. 7, figs. 2–3.
Note: Most *Gt. minuta* at Leg 139 sites do not have a bulla. The ampulate form of *Gt. minuta* (Natland) as illustrated in fig. 2.7k of Hemleben et al. (1989) is rare in Leg 139 samples. The form is gradational with *Gt. uvula* and was grouped with the *Gt. uvula* counting group during the census.

Globigerinita uvula (Ehrenberg)
Pylodexia uvula Ehrenberg, 1861, p. 206, 207, 308.
Note: The group includes a low spired form intermediate between *Gt. uvula* and *Gt. minuta* referred to *Gt.* cf. *uvula.* All three taxa are included in the *Gt. uvula* counting group tabulated in the census.

Globigerinoides ruber (d'Orbigny)
Globigerina ruber d'Orbigny, 1839a, p. 82; v. 8, pl. 4, figs. 12–14.

Globorotalia hirsuta (d'Orbigny)
Rotalina hirsuta d'Orbigny, 1839b, p. 131, pl.1, figs. 34–36.

Globorotalia inflata (d'Orbigny)
Globigerina inflata d'Orbigny, 1839b, p. 134, pl. 12, figs 7–9.

Globorotalia scitula (Brady)
Pulvinulina scitula Brady, 1882, p. 716; figured in Brady, 1884, pl. 103, figs. 7a–c.

Globorotalia theyeri Fleisher
Globorotalia theyeri Fleisher, 1974, p. 1028, pl. 12, fig. 9; pl. 13, figs. 1–5.

Globoturborotalita rubescens (Hofker)
Globigerina rubescens Hofker, 1956, v. 15, p. 234, pl. 32, fig. 26, pl. 35, figs. 18–21.

Neogloboquadrina pachyderma (Ehrenberg)
Aristospira pachyderma Ehrenberg, 1861, p. 276, 277, and 303.
Note: Most sinistral coiling forms are the encrusted Group A variety of Reynolds and Thunell (1986) and Form 1 of Keller (1978), and most dextral coiling forms are the reticulate and lobate Group B variety of Reynolds and Thunell (1986) and Forms 2 and 3 of Keller (1978).

Orbulina universa d'Orbigny
Orbulina universa d'Orbigny, 1839a, p. 3, pl. 1, fig. 1.

Tenuitella iota (Parker)
Globigerinita iota Parker, 1962, p. 250–252, pl. 10, figs. 26–30.

Tenuitella parkerae (Brönnimann and Resig)
Globorotalia parkerae Brönnimann and Resig, 1971, p. 1280–1281, pl. 43, figs. 7, 10; pl. 47, figs. 4, 6; pl. 48, figs. 2–3.

Turborotalita humilis (Brady)
Truncatulina humilis Brady, 1884, p. 665, pl. 94, fig. 7.

Turborotalita quinqueloba (Natland)
Globigerina quinqueloba Natland, 1938, p. 149, pl. 6, fig. 7.
Note: The *Ga. quinqueloba* group consists of *Ga. quinqueloba* Natland and *Ga. clarkei* (Rögl and Bolli), two taxa that are difficult to distinguish as discussed in Hemleben et al. (1989), p. 13.

ACKNOWLEDGMENTS

I heartily thank R. Timothy Patterson and an anonymous reviewer for their helpful comments that improved this manuscript. I especially want to acknowledge and thank my colleagues on board Leg 139 for the open exchange of ideas and data which provided the context for this

Table 7. Species composition (relative frequency %) of clusters.

Sample	Pdl	Pdr	Bul	Qui	Glu	Uvu	Tran
Cluster 1a							
856A-6H-6, 46–48	73	0	1	4	0	18	0
856A-6H-6, 112–114	74	0	1	5	0	18	0
856A-6H-3, 127–129	72	0	1	5	1	18	0
856A-7H-2, 12–14	69	0	4	4	1	19	0
856A-4H-7, 62–64	67	1	2	10	1	18	0
856A-5H-7, 88–90	68	0	0	7	0	24	0
857A-8H-5, 40–44	63	0	4	8	1	24	0
856A-4H-2, 81–83	67	2	9	6	1	15	0
856A-4H-3, 122–124	69	1	6	7	0	14	2
856A-4H-4, 88–90	63	6	0	19	0	13	0
856A-2H-6, 86–88	59	1	10	8	3	17	0
857A-2H-5, 22–24	58	0	7	14	2	18	0
856A-4H-1, 82–84	61	3	2	11	2	17	3
857A-5H-4, 9–13	62	7	1	9	6	14	0
857A-2H-1, 105–107	71	1	5	12	1	8	0
857A-4H-5, 40–44	66	1	8	15	3	6	0
857A-4H-4, 70–74	71	3	4	14	6	2	1
857A-8H-1, 119–123	58	0	14	16	1	7	0
856A-4H-6, 108–110	82	1	3	4	2	8	0
856A-6H-2, 123–125	86	0	0	4	0	7	0
856A-4H-5, 96–98	77	3	6	7	1	6	0
Cluster 1b							
856A-5H-3, 135–137	61	0	0	9	0	30	0
856A-6H-1, 68–70	57	1	0	7	1	32	1
856A-5H-5, 133–135	53	1	0	11	0	33	0
856A-7H-1, 48–50	48	0	0	10	0	40	0
857A-2H-1, 97–99	50	1	5	19	0	20	0
857A-2H-6, 9–11	53	1	6	20	1	18	0
857A-2H-4, 12–14	48	1	3	23	2	22	0
856A-5H-4, 88–90	47	0	6	15	1	25	0
857A-8H-2, 21–25	49	0	7	16	0	23	0
857A-9H-4, 60–63	45	0	11	19	2	22	0
856A-2H-2, 90–92	54	1	8	21	3	11	0
856A-1H-1, 0–1	44	8	8	15	5	13	1
857A-4H-3, 64–66	52	1	26	4	1	13	0
Cluster 2							
856A-3H-5, 78–80	1	3	3	64	6	17	0
857A-5H-5, 140–142	0	5	3	61	8	14	3
856A-3H-5, 130–132	2	4	1	43	6	34	3
857A-5H-5, 105–107	1	7	1	39	12	31	4
856A-3H-5, 74–76	3	7	0	40	9	21	2
856A-3H-5, 96–98	1	4	2	48	7	20	1
Cluster 3c							
857A-1H-1, 0–1	16	3	8	19	3	50	0
857A-1H-3, 10–13	16	0	10	18	2	50	0
856A-1H-1, 91–93	14	0	3	21	3	53	0
857A-8H-7, 22–26	18	0	4	24	1	53	0
857A-1H-5, 89–91	16	0	8	20	8	41	0
857A-1H-1, 79–81	28	1	18	6	1	40	0
857A-1H-2, 125–129	22	0	18	11	6	42	0
857A-7H-7, 28–32	33	1	4	11	1	35	0
857A-8H-3, 54–58	39	0	8	11	0	38	0
857A-8H-5, 114–118	29	0	7	15	1	46	0
857A-10H-1, 124–127	31	0	7	14	2	45	0
857A-10H-2, 12–14	30	0	8	13	0	48	0
857A-2H-7, 26–28	31	1	5	11	3	46	0
857A-1H-6, 36–38	27	0	5	18	4	42	0
857A-8H-6, 52–56	27	0	5	18	2	46	0
856A-5H-2, 6–8	39	0	0	16	0	45	0
857A-8H-4, 43–47	24	0	5	11	1	56	0
Cluster 3b							
857A-5H-4, 57–61	19	7	8	39	3	15	7
857A-5H-4, 130–132	24	7	7	38	4	15	1
857A-5H-4, 70–72	27	11	13	34	3	9	0
856A-2H-5, 86–88	40	1	14	27	3	14	0
857A-2H-2, 20–22	38	0	15	27	1	19	0
857A-4H-4, 12–14	40	5	15	27	4	8	0
857A-4H-4, 30–32	30	1	23	28	3	12	0
Cluster 3a							
857A-6H-2, 76–80	20	1	13	32	2	30	0
857A-6H-3, 27–31	15	0	12	35	2	33	0
856A-5H-1, 19–21	16	0	7	33	2	26	0
857A-4H-4, 38–40	16	2	16	28	6	30	1
857A-6H-5, 4–8	15	0	7	32	1	39	0
857A-6H-4, 66–70	7	0	9	39	4	37	1
856A-3H-4, 91–93	27	4	11	30	2	23	0
857A-4H-5, 127–129	30	0	12	31	3	19	0
857A-2H-4, 127–129	32	0	9	29	2	26	0
857A-6H-1, 59–63	28	0	8	28	2	33	0
857A-7H-4, 1–5	25	0	6	30	2	33	0
857A-7H-4, 85–89	25	1	9	25	1	34	0
857A-7H-3, 37–39	30	0	8	24	1	35	0
857A-5H-2, 13–17	31	1	2	28	3	32	0
856A-3H-6, 92–94	27	1	3	22	1	42	0
857A-2H-4, 98–100	30	0	4	24	2	39	0
857A-9H-3, 74–80	23	0	4	25	1	45	0
857A-2H1, 45–48	23	0	9	23	3	40	0
857A-2H-3, 98–100	39	1	7	17	5	30	0
857A-2H-5, 7–9	36	0	9	20	6	28	0
857A-7H-5, 75–79	35	1	6	24	1	30	0
857A-7H-6, 121–125	40	0	7	21	0	30	0
856A-2H-4, 101–103	41	1	6	23	2	22	1
856A-2H-3, 90–92	39	1	13	17	6	21	2
856A-3H-3, 72–74	31	0	22	21	2	22	0
857A-2H-3, 129–131	28	0	20	22	2	26	0
857A-2H-2, 129–131	31	0	12	23	3	31	0
857A-10H-4, 99–101	27	0	14	24	2	30	0
857A-6H-7, 38–42	27	1	14	24	3	24	0
856A-1H-2, 48–50	35	1	12	17	3	31	0
856A-2H-7, 56–58	33	1	14	20	2	30	0
857A-2H-2, 96–98	29	0	10	18	4	34	0
857A-9H-5, 79–84	28	1	13	20	1	33	0
857A-4H-7, 43–47	25	1	17	18	4	30	1
856A-9H-6, 46–48	32	0	20	13	10	23	0
857A-4H-3, 125–127	40	1	18	9	2	24	2
856A-3H-4, 117–119	13	17	10	18	5	30	5
857A-4H-4, 49–51	29	8	32	12	5	11	0
857A-1H-4, 72–76	21	0	0	71	0	7	0

Notes: Pdl = sinistral *Neogloboquadrina pachyderma*; Pdr = dextral *Neogloboquadrina pachyderma*; Bul = *Globigerina bulloides*; Qui = *Turborotalita quinqueloba*; Glu = *Globigerinita glutinata*; Uvu = *Globigerinita uvula* group; Tran = transitional/cool subtropical species including *Globorotalia hirsuta, Globorotalia inflata, Globigerinoides ruber, Globoturborotalita rubescens, Turborotalita humilis, Tenuitella iota, Orbulina universa.*

Table 8. Mean species composition (%) and standard deviation of cluster assemblages.

Cluster	Pdl	Pdr	Bul	Qui	Glu	Uvu	Tran
1b	68 ± 7	1 ± 2	4 ± 4	9 ± 4	2 ± 2	14 ± 6	0 ± 1
1a	51 ± 5	1 ± 2	6 ± 7	15 ± 6	1 ± 1	23 ± 8	0 ± 0
2	1 ± 1	5 ± 2	2 ± 1	49 ± 10	8 ± 2	23 ± 7	2 ± 1
3c	26 ± 7	0 ± 1	7 ± 5	15 ± 5	2 ± 2	46 ± 5	0 ± 0
3b	31 ± 8	5 ± 4	14 ± 5	31 ± 5	3 ± 1	13 ± 4	1 ± 2
3a	28 ± 8	1 ± 3	11 ± 6	24 ± 6	3 ± 2	30 ± 7	0 ± 1

Notes: Pdl = sinistral *Neogloboquadrina pachyderma*; Pdr = dextral *Neogloboquadrina pachyderma*; Bul = *Globigerina bulloides*; Qui = *Turborotalita quinqueloba*; Glu = *Globigerinita glutinata*; Uvu = *Globigerinita uvula* group; Tran = Transitional/cool subtropical species including *Globorotalia hirsuta, Globorotalia inflata, Globigerinoides ruber, Globoturborotalita rubescens, Turborotalita humilis, Tenuitella iota, Orbulina universa.*

work. Thanks also to the able and competent crew on board the *Resolution* and the excellent editorial staff at ODP. Ms. Susan Moffett prepared samples, maintained the sample database, and assisted in the microscopic analysis. Mr. Zhongbo Yu assisted in preparation of samples and completed the sample database. The onshore study was supported in part by a grant from the JOI/U.S. Science Support Program.

REFERENCES*

Al-Aasm, I.S., and Blaise, B., 1991. Interaction between hemipelagic sediment and a hydrothermal system: Middle valley, northern Juan de Fuca ridge, subarctic northeast Pacific. *Mar. Geol.*, 98:25–40.

Bandy, O.L., 1960. The geological significance of coiling ratios in the foraminifer *Globigerina pachyderma* (Ehrenberg). *J. Paleontol.*, 34:671–681.

* Abbreviations for names of organizations and publications in ODP reference lists follow the style given in *Chemical Abstracts Service Source Index* (published by American Chemical Society).

Berger, W.H., 1976. Biogenous deep-sea sediments: production, preservation, and interpretation. *In* Riley, J.P., and Chester, R. (Eds.), *Chemical Oceanography* (Vol. 5): San Diego (Academic Press), 266–389.

————, 1981. Paleoceanography: the deep-sea record. *In* Emiliani, C. (Ed.), *The Sea* (Vol. 7): *The Oceanic Lithosphere:* New York (Wiley), 1437–1519.

Blow, W.H., 1959. Age, correlation, and biostratigraphy of the upper Tocuyo (San Lorenzo) and Pozón Formations, Eastern Falcón, Venezuela. *Bull. Am. Paleontol.,* 39:67–251.

Bradshaw, J.S., 1959. Ecology of living planktonic foraminifera in the north and equatorial Pacific Ocean. *Contrib. Cushman Found. Foraminiferal Res.,* 10:25–64.

Brady, H.B., 1882. Report on the Foraminifera. *In* Tizard and Murray (Eds.), *Exploration of the Faröe Channel During the Summer of 1880, in Her Majesty's Hired Ship "Knight Errant."* Proc. R. Soc. Edinburgh, 11:708–717.

————, 1884. Report on the Foraminifera dredged by H.M.S. *Challenger,* during the years 1873–1876. *Rep. Sci. Results Challenger Exped., Zool.,* 9:1–814.

Brönnimann, P., and Resig, J., 1971. A Neogene globigerinacean biochronologic time-scale of the Southwestern Pacific. *In* Winterer, E.L., Riedel, W.R., et al., *Init. Repts. DSDP,* 7 (Pt. 2): Washington (U.S. Govt. Printing Office), 1235–1469.

Brunner, C.A., and Ledbetter, M., 1987. Sedimentological and micropaleontological detection of turbidite muds in hemipelagic sequences: an example from the late Pleistocene levee of Monterey Fan, central California continental margin. *Mar. Micropaleontol.,* 12:223–239.

————, 1989. Late Quaternary quantitative planktonic foraminiferal biostratigraphy in turbidite sequences of the central California continental margin. *Micropaleontology,* 35:321–336.

Coulbourn, W.T., Parker, F.L., and Berger, W.H., 1980. Faunal and solution patterns of planktonic foraminifera in surface sediments of the North Pacific. *Mar. Micropaleontol.,* 5:329–399.

Davis, E.E., Mottl, M.J., Fisher, A.T., et al., 1992. *Proc. ODP, Init. Repts.,* 139: College Station, TX (Ocean Drilling Program).

d'Orbigny, A.D., 1826. Tableau méthodique de la classe des céphalopodes. *Annales des Sciences Naturelles,* Paris, Ser. 1, 7:245–314.

————, 1839a. Foraminifères. *In* de la Sagra, R. (Ed.), *Histoire Physique, Politique et Naturelle de L'île de Cuba:* Paris (Arthus Bertrand), 8:1–224 [plates published separately].

————, 1839b. Foraminifères des iles Canaries. *In* Barker-Webb, P., and Berthelot, S. (Eds.), *Historie Naturelle des Iles Canaries* (Vol. 2): Paris (Béthune), 119–146.

Duncan, J.R., Fowler, G.A., and Kulm, L., 1970. Planktonic foraminiferal-radiolarian ratios and Holocene-late Pleistocene deep sea stratigraphy off Oregon. *Geol. Soc. Am. Bull.,* 81:561–566.

Egger, J.G., 1893. Foraminiferen aus Meeresgrundproben, gelothet von 1874 bis 1876 von S. M. Sch. Gazelle. *Abh. Bayerischen Akad. Wiss., München, Math.-Physik. Cl.,* 18:193–458.

Ehrenberg, C.G., 1861. Elemente des tiefen Meeresgrundes im Mexikanischen Golfstrome bei Florida; über die Tiefgrund-Verhältnisse des Oceans am Eingange der Davisstrasse und bei Island. *K. Preuss. Akad. Wiss. Berlin Monatsber.,* 275–315.

Favorite, F., Dodimead, A.J., and Nasu, K., 1976. Oceanography of the Subarctic Pacific Region, 1960–71. *Internat. N. Pac. Fisheries Comm. Bull.,* 33:1–187.

Fleisher, R.L., 1974. Cenozoic planktonic foraminifera and biostratigraphy, Arabian Sea, Deep Sea Drilling Project, Leg 23A. *In* Whitmarsh, R.B., Weser, O.E., Ross, D.A., et al., *Init. Repts. DSDP,* 23: Washington (U.S. Govt. Printing Office), 1001–1072.

Gardner, J.V., Heusser, L.E., Quinterno, P., Stone, S.M., Barron, J.A., and Poore, R.Z., 1988. Clear Lake record vs. the adjacent marine record: a correlation of their past 20,000 years of paleoclimatic and paleoceanographic responses. *In* Sims, J.D. (Ed.), *Late Quaternary Climate, Tectonism, and Sedimentation in Clear Lake, Northern California Coast Ranges.* Spec. Pap.—Geol. Soc. Am., 214:171–182.

Hays, J.D., and Shackleton, N.J., 1976. Globally synchronous extinction of the radiolarian *Stylatractus universus. Geology,* 4:649–652.

Hemleben, C., Spindler, M., and Anderson, O.R., 1989. *Modern Planktonic Foraminifera:* New York (Springer-Verlag).

Hofker, J., 1956. Foraminifera of Santa Cruz and Thatch-Island, Virginia Archipelago, West Indies. *Copenhagen Univ., Zool. Mus. Spolia (Skrifler),* 15:234.

Ingle, J.C., Jr., 1973a. Neogene foraminifera from the northeastern Pacific Ocean, Leg 18, Deep Sea Drilling Project. *In* Kulm, L.D., von Huene, R., et al., *Init. Repts. DSDP,* 18: Washington (U.S. Govt. Printing Office), 517–567.

————, 1973b. Summary comments on Neogene biostratigraphy, physical stratigraphy, and paleo-oceanography in the marginal northeastern Pacific Ocean. *In* Kulm, L.D., von Huene, R., et al., *Init. Repts. DSDP,* 18: Washington (U.S. Govt. Printing Office), 949–960.

Karlin, R., and Lyle, M., 1986. Sediment studies of the Gorda Ridge. Final Report for Contract No. 63-630-8508, Oregon Department of Geology and Mineral Industries and the Gorda Ridge Technical Task Force, *Open-File Rep.,* O-86-19.

Karlin, R., Lyle, M., and Zahn, R., 1992. Carbonate variations in the northeast Pacific during the late Quaternary. *Paleoceanography,* 7:43–61.

Keller, G., 1978. Morphologic variation of *Neogloboquadrina pachyderma* (Ehrenberg) in sediments of the marginal and central northeast Pacific Ocean and paleoclimatic interpretation. *J. Foraminiferal Res.,* 8:208–224.

Kent, D., Opdyke, N.D., and Ewing, M., 1971. Climatic change in the North Pacific using ice-rafted detritus as a climatic indicator. *Geol. Soc. Am. Bull.,* 82:2741–2754.

Kheradyar, T., 1992. Pleistocene planktonic foraminiferal assemblages and paleotemperature fluctuations in Japan Sea, Site 798. *In* Pisciotto, K.A., Ingle, J.C., Jr., von Breymann, M.T., Barron, J., et al., *Proc. ODP, Sci. Results,* 127/128 (Pt. 1): College Station, TX (Ocean Drilling Program), 457–470.

Krumbein, W.C., and Pettijohn, F.J., 1938. *Manual of Sedimentary Petrography:* New York (Appleton-Century-Crofts).

Lagoe, M.B., and Thompson, P.R., 1988. Chronostratigraphic significance of late Cenozoic planktonic foraminifera from the Ventura Basin, California: potential for improving tectonic and depositional interpretation. *J. Foraminiferal Res.,* 18:250–266.

Langer, M.R., 1992. Biosynthesis of glycosaminoglycans in foraminifera: a review. *Mar. Micropaleontol.,* 19:245–255.

Lyle, M., Zahn, R., Prahl, F., Dymond, J., Collier, R., Pisias, N., and Suess, E., 1992. Paleoproductivity and carbon burial across the California Current: the Multitracers Transect, 42°N. *Paleoceanography,* 7:251–272.

Moore, T.C., Jr., Burckle, L.H., Geitzenauer, K., Luz, B., Molina-Cruz, A., Robertson, J.H., Sachs, H., Sancetta, C., Thiede, J., Thompson, P., and Wenkam, C., 1980. The reconstruction of sea surface temperatures in the Pacific Ocean of 18,000 B.P. *Mar. Micropaleontol.,* 5:215–247.

Natland, M.L., 1938. New species of Foraminifera from off the West Coast of North America and from the later Tertiary of the Los Angeles Basin. *California Univ. Scripps Inst. Oceanogr. Bull. Tech. Ser.,* 4:137–164.

Nayudu, Y.R., 1964. Carbonate deposits and paleoclimatic implications in the northeast Pacific Ocean. *Science,* 146:515–517.

Nelson, C.H., Kulm, L.D., Carlson, P.R., and Duncan, J.R., 1968. Mazama Ash in the northeastern Pacific. *Science,* 161:47–49.

Olsson, R.K., and Goll, R., 1970. Biostratigraphy. *In* McManus, D.A., Burns, R.E., et al., *Init. Repts. DSDP,* 5: Washington (U.S. Govt. Printing Office), 557–567.

Parker, F.L., 1962. Planktonic foraminiferal species in Pacific sediments. *Micropaleontology,* 8:219–254.

Reynolds, L., and Thunell, R.C., 1985. Seasonal succession of planktonic foraminifera in the subpolar North Pacific. *J. Foraminiferal Res.,* 15:282–301.

————, 1986. Seasonal production and morphologic variation of *Neogloboquadrina pachyderma* (Ehrenberg) in the northeast Pacific. *Micropaleontology,* 32:1–18.

Rögl, F., and Bolli, H.M., 1973. Holocene to Pleistocene planktonic foraminifera of Leg 15, Site 147 (Cariaco Basin [Trench], Caribbean Sea) and their climatic interpretation. *In* Edgar, N.T., Saunders, J.B., et al., *Init. Repts. DSDP,* 15: Washington (U.S. Govt. Printing Office), 553–615.

Sancetta, C.A., 1979. Oceanography of the North Pacific during the last 18,000 years: evidence from fossil diatoms. *Mar. Micropaleontol.,* 4:103–123.

Sautter, L.R., and Sancetta, C.A., 1992. Seasonal associations of phytoplankton and planktic foraminifera in an upwelling region and their contribution to the seafloor. *Mar. Micropaleontol.,* 18:263–278.

Sautter, L.R., and Thunell, R.C., 1989. Seasonal succession of planktonic foraminifera: results from a four-year time-series sediment trap experiment in the northeast Pacific. *J. Foraminiferal Res.,* 19:253–267.

————, 1991. Planktonic foraminiferal response to upwelling and seasonal hydrographic conditions: sediment trap results from San Pedro Basin, Southern California Bight. *J. Foraminiferal Res.,* 21:347–363.

Sidner, B.R., and McKee, T.R., 1976. Geochemical controls on vertical distribution of iron-rich agglutinated foraminifers in late Quaternary continental slope sediments from northwest Gulf of Mexico. *AAPG Bull.,* 60:722–723.

Stow, D.A.V., and Piper, D.J.W., 1984. *Fine-Grained Sediments: Deep-Water Processes and Facies:* London (Blackwell Sci. Publ.).

Sverdrup, H.U., Johnson, M.W., and Fleming, R.H. (Eds.), 1942. *The Oceans: Their Physics, Chemistry and General Biology:* Englewood Cliffs, NJ (Prentice-Hall).

Thompson, P.R., 1980. Foraminifers from Deep Sea Drilling Project Sites 434, 435, and 436, Japan Trench. *In* von Huene, R., and Nasu, N., et al., *Init. Repts. DSDP,* 56, 57 (Pt. 2): Washington (U.S. Govt. Printing Office), 775–807.

————, 1981. Planktonic foraminifera in the western North Pacific during the past 150,000 years: comparison of modern and fossil assemblages. *Palaeogeogr., Palaeoclimatol., Palaeoecol.,* 35:241–279.

Thompson, P.R., and Shackleton, N.J., 1980. North Pacific paleoceanography: late Quaternary coiling variations of planktonic foraminifer *Neogloboquadrina pachyderma. Nature,* 287:829–833.

Zahn, R., Rushdi, A., Pisias, N.G., Bornhold, B.D., Blaise, B., and Karlin, R., 1991. Carbonate deposition and benthic del-^{13}C in the subarctic Pacific: implications for changes of the oceanic carbonate system during the past 750,000 years. *Earth Planet. Sci. Lett.,* 103:116–132.

Date of initial receipt: 21 January 1993
Date of acceptance: 8 June 1993
Ms 139SR-206

Table 9. Dendrogram of results of Q-mode cluster analysis.

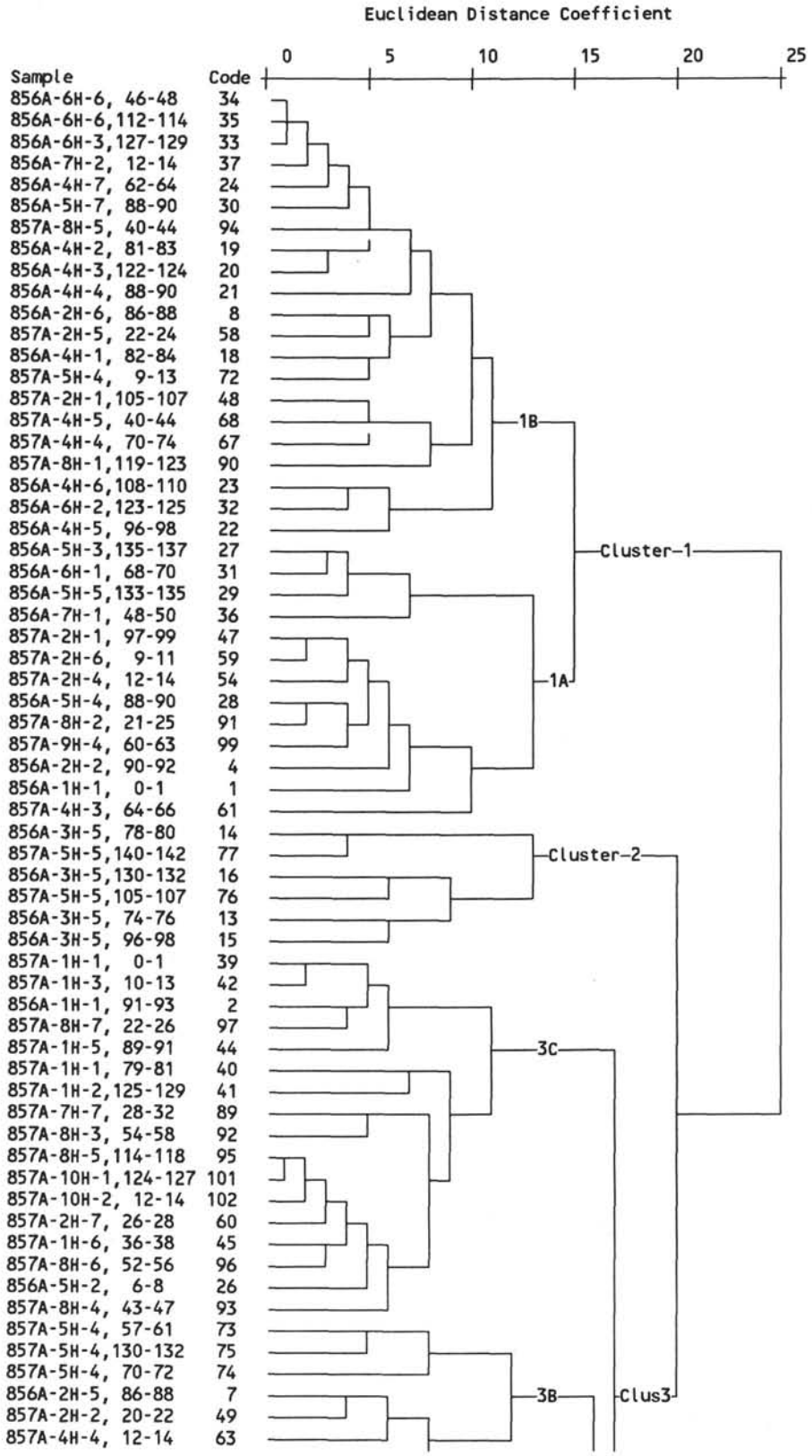

Table 9 (continued).

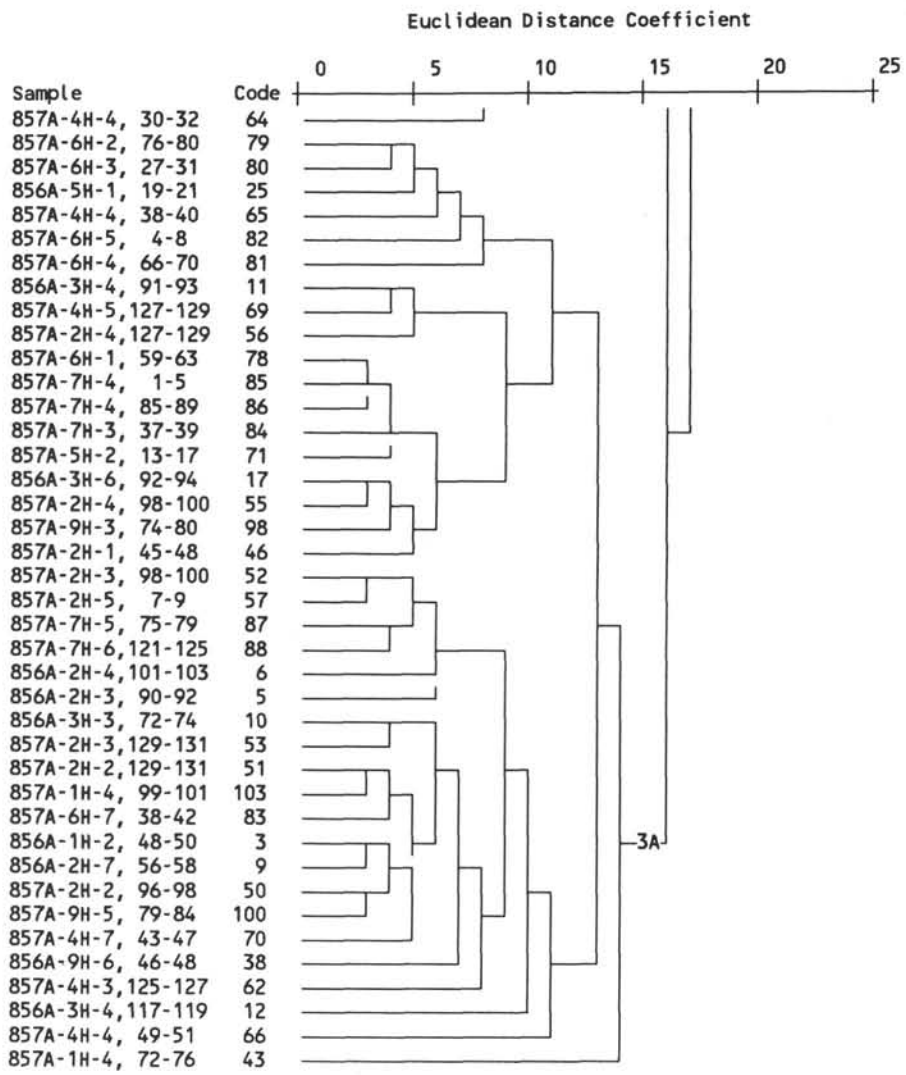

Table 10. Correlation analysis, matrix of correlation coefficients.

Correlation Matrix	Sinistral *Nq. pachyderma*	Dextral *Nq. pachyderma*	Ga. *bulloides*	Tr. *quinqueloba*	*Gt. glutinata*	*Gt. uvula*	Transitional spp.
Sinistral *Nq. pachyderma*	1.00						
Dextral *Nq. pachyderma*	–0.20	1.00					
Ga. bulloides	–0.22	0.03	1.00				
Tr. quinqueloba	–0.72*	0.23	–0.05	1.00			
Gt. glutinata	–0.48*	0.43*	0.16	0.38*	1.00		
Gt. uvula	–0.52*	–0.031*	–0.10	–0.04	–0.07	1.00	
Transitional spp.	–0.26	0.59*	–0.09	0.27	0.40*	–0.13	1.00

Notes: * = one-tailed significance of 0.001; number of cases = 103.

Table 11. Sedimentation rates based on tentative correlations.

Coiling direction zone	Hole 856A Depth of base (mbsf)	Hole 856A Tentative age (yr)	Hole 856A Sed. rate ($cm/10^3 yr$)	Hole 857A Depth of base (mbsf)	Hole 857A Tentative age (yr)	Hole 857A Sed. rate ($cm/10^3$ yr)
CD1	0.46 ± 0.46 m	11,000	4	2.31 ± 0.40 m	11,000	21
Unzoned	—	—	—	26.94 ± 0.05 m	?	?
CD3	20.06 ± 0.56 m	125,000	17	40.37 ± 0.21 m	125,000	33